


Article

# Vanadium(V) Removal from Aqueous Solutions and Real Wastewaters onto Anion Exchangers and Lewatit AF5

Anna Wołowicz \*  and Zbigniew Hubicki

Department of Inorganic Chemistry, Faculty of Chemistry, Institute of Chemical Sciences, Maria Curie-Skłodowska University, Maria Curie-Skłodowska Square 2, 20-031 Lublin, Poland  
\* Correspondence: anna.wolowicz@mail.umcs.pl; Tel.: +48-81-537-57-27

**Abstract:** Adsorption abilities of weakly (Purolite A830), weakly basic/chelating (Purolite S984), and strongly basic (Lewatit MonoPlus SR7, Purolite A400TL, Dowex PSR2, Dowex PSR3) ion exchange resins of different functional groups and microporous Lewatit AF5 without functional groups towards vanadium(V) ions were studied in batch and column systems. In the batch system, the influence of the sorbent mass (0.01–0.1 g), pH (2–10), the phase contact time (1–1440 min), and the initial concentration (5–2000 mg/L) were studied, whereas in the column system, the initial concentrations (50, 100, and 200 mg/L) with the same bed volume and flow rate (0.4 mL/min) were studied. Desorption agents HCl and NaOH of 0.1–1 mol/L concentration were used for loaded sorbent regeneration. The pseudo-first order, pseudo-second order and intraparticle diffusion kinetic models as well as the Langmuir, Freundlich, Temkin, and Dubinin–Radushkevich isotherm models were used to describe kinetic and equilibrium data to acquire improved knowledge on the adsorption mechanism. The desorption efficiency was the largest using 0.5 mol/L NaOH for all sorbents under discussion. Purolite S984, Purolite A830, and Purolite A400TL, especially Purolite S984, are characterized by the best removal ability towards vanadium(V) from both model and real wastewater.

**Keywords:** vanadium; removal; ion exchange resin; wastewater; adsorption



**Citation:** Wołowicz, A.; Hubicki, Z. Vanadium(V) Removal from Aqueous Solutions and Real Wastewaters onto Anion Exchangers and Lewatit AF5. *Molecules* **2022**, *27*, 5432. <https://doi.org/10.3390/molecules27175432>

Academic Editors: Maciej Thomas and Susan J. Masten

Received: 5 August 2022

Accepted: 22 August 2022

Published: 25 August 2022

**Publisher's Note:** MDPI stays neutral with regard to jurisdictional claims in published maps and institutional affiliations.



**Copyright:** © 2022 by the authors. Licensee MDPI, Basel, Switzerland. This article is an open access article distributed under the terms and conditions of the Creative Commons Attribution (CC BY) license (<https://creativecommons.org/licenses/by/4.0/>).

## 1. Introduction

Vanadium(V) is a contaminant in wastewater as a result of the economy and industry development as well as increasing consumption year after year (Figure 1). Its enormous application in many fields of industry as well as the mining, smelting, and processing of ores containing vanadium are the main sources of vanadium in the environment (Figure 1) [1].

The effluent discharge containing a large concentration of vanadium and its potential toxicity can be dangerous for animals and human [2]. Therefore, increasing attention has focused on the removal of vanadium from water and wastewater to control its concentration in the environment as well as for its recovery. Adsorption, chemical precipitation, solvent extraction, electrokinetic remediation, photocatalysis reduction, coagulation, microbiological treatment, and membrane filtration methods have been developed to remove vanadium from wastewater. The main advantages and disadvantages of the mentioned technique are presented in Figure 2 [3]. In recent years, adsorptions underwent rapid development and became a great potential method for heavy metal removal and separation. Brief consumption, fast kinetics, great effectiveness, technological simplicity, small energy consumption, environmental friendliness as well as the availability of a wide range of adsorbents and possibility of its regeneration render adsorption one of the most frequently applied techniques for vanadium removal [1–4]. Ion exchange resins, oxides, biosorbents, nanomaterials, and iron-based or hybrid materials were applied for vanadium removal and separation. They are discussed in the literature and take into account solution pH, co-existing ions, contact time, sorbent dosage, temperature, adsorption mechanism, etc. [1–3].

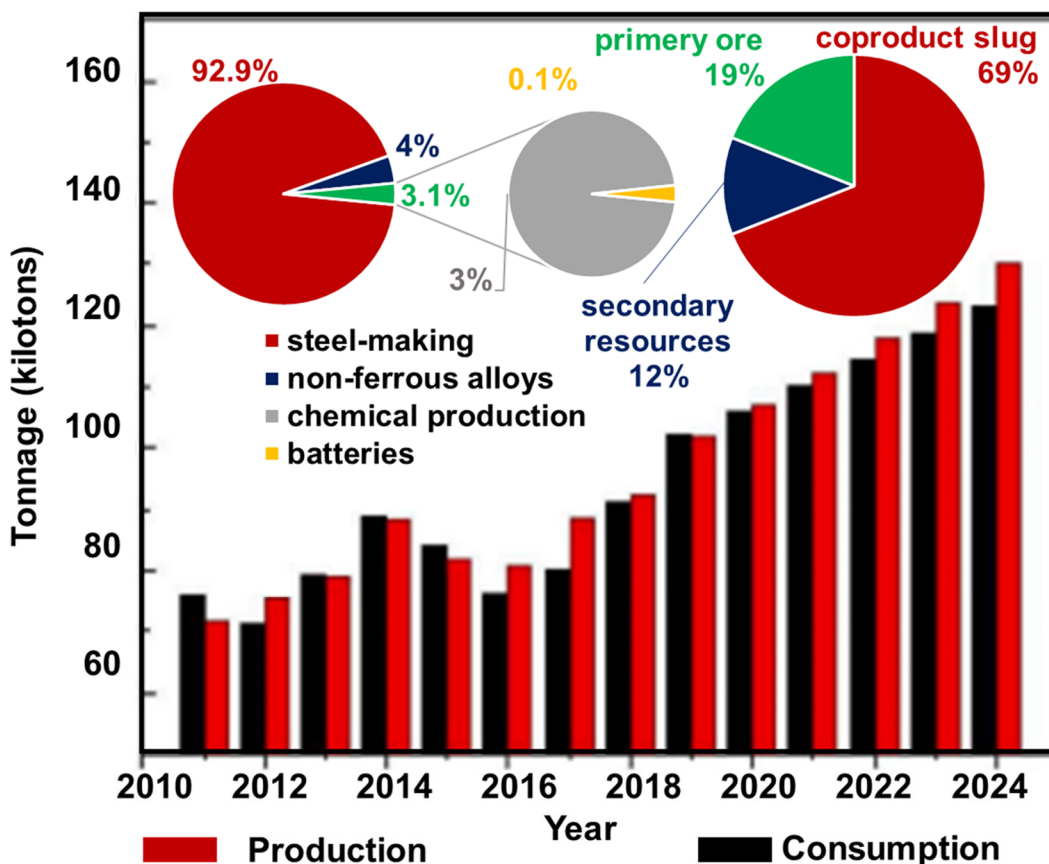


Figure 1. Global vanadium production and consumption in 2010–2025; the sources of vanadium production and branches of industry using vanadium.

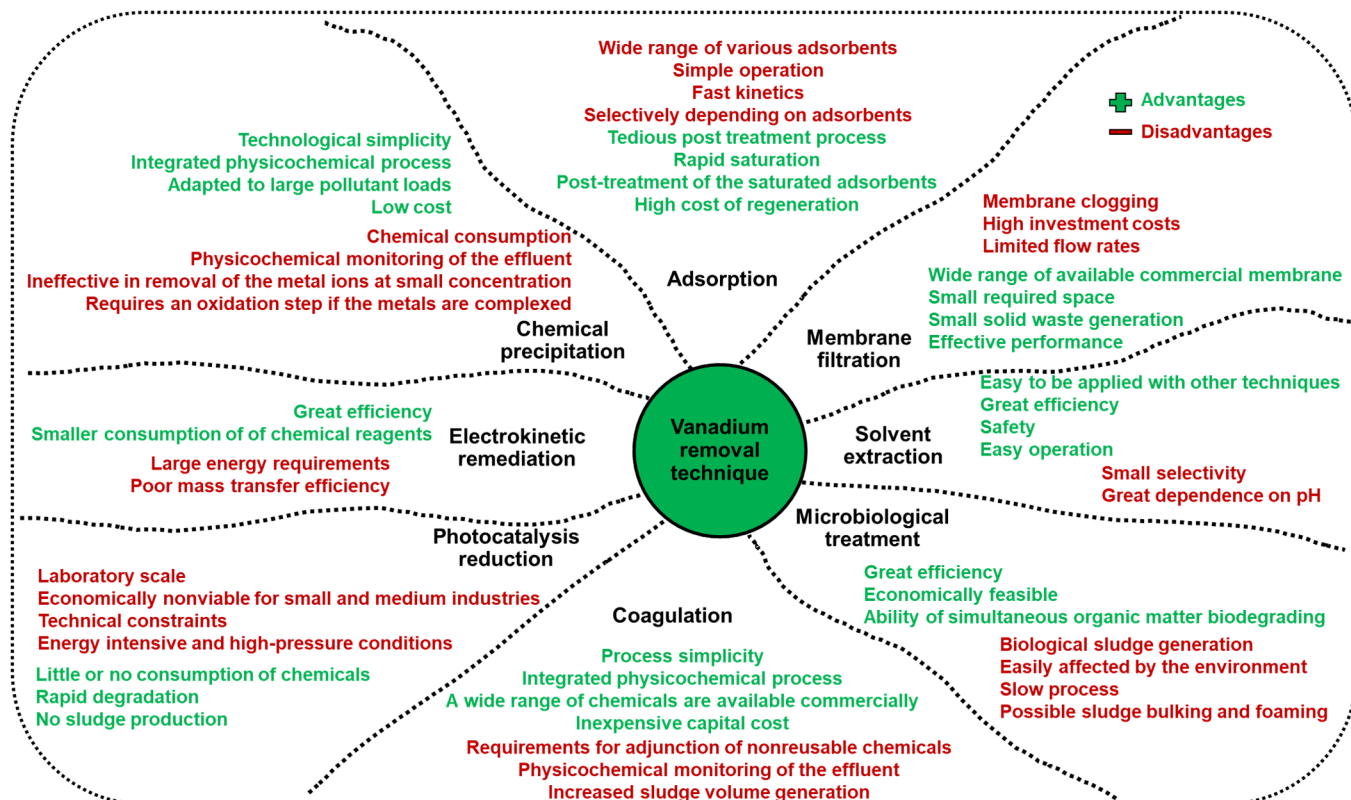


Figure 2. Comparison of treatment technologies for the vanadium removal from wastewaters.

Of the commercially available sorbents, ion exchange resins are often used for vanadium removal due to their characteristics of easy operation, small chemical consumption, good flexibility, and versatility [2]. The strongly (Amberlite IRA-400 [5,6], D201, 717 [7], and D296 [8]) and weakly (Amberlite IRA-743 [5], D314 [7,9], ZGA414 [10]) basic anion exchange resins and chelating (Lewatit MonoPlus TP220, Dowex M4195 [11], DDAS, CUW or CW-2 [12]) resins have been applied for vanadium removal in the past [5–12].

The strongly (Amberlite IRA-400) and weakly (Amberlite IRA-743) basic ion-exchange resins were applied for the V(V) and Mo(VI) sorption. The sorption capacity was 208 and 177 mg/L for Amberlite IRA-743 (pH = 4.0) and Amberlite IRA-400 (pH = 6). The sorption process was endothermic [5]. Due to numerous co-properties in the chemistry of molybdenum and vanadium, the separation of these elements is difficult but the D296 resin could be effectively applied for separation in the pH range of 6.5–8.5. The chloride ions affect the separation significantly. When the concentration of the chloride ions is close to 70 g/L, it is impossible to remove vanadium from the solution with D296. The effective regeneration of the loaded strongly basic anion exchange resin over 98.5% was obtained using 6 mol/L HCl. The resin adsorbed  $V_3O_9^{3-}$  preferentially due to higher charges contained in  $V_3O_9^{3-}$  than that in  $MoO_4^{2-}$  in the ammonium molybdate solution (pH = 7.14) [8]. Amberlite IRA-400 was also applied for vanadium removal and recovery from the alkaline steel slag leachates at pH 11.5. The sorption kinetics followed the pseudo-first order kinetic model and the maximum adsorption capacity was 27 mg/L. The great anion exchange resin efficiency was also proved in column studies and the desorption yield was 57–72% with 2 mol/L NaOH. The reuse studies showed that this resin could be reused 20 times without a capacity reduction and with 69% of V recovery during the regeneration [6]. Strongly D201, 717, and D296 and weakly ZGA414 and D314 basic anion exchange resins with high efficiency were also confirmed during the vanadium extraction from the hydrochloric acid leaching solution of red mud [7] and from the sulfuric acid leach solutions of stone coals [8–10]. More than 99% of vanadium was selectively adsorbed by the D201 resin (pH 2.0, flow speed of  $6 \text{ m}^3/\text{h}\cdot\text{m}^3$ ), D314 (pH 3.0, flow speed of  $4.8 \text{ m}^3/\text{h}\cdot\text{m}^3$ ), and 717 (pH 5.0, flow speed of  $7.92 \text{ m}^3/\text{h}\cdot\text{m}^3$ ) [7] as well as D314 (2.06 g/L ( $V_2O_5$ ), 260 mg/mL, contact time of 60 min, pH 4) [9]. The adsorption process of vanadium follows the pseudo-second order kinetic model [7]. The separation of vanadium from the solution containing Fe(III), Fe(II), Al(III), and Mg(II) ions by the ion exchange and the solvent extraction indicated that only V(V) was loaded from the synthetic solution by ZGA414 at pH > 1.5, and after the reduction to V(IV), vanadium was extracted with 99% efficiency [10].

Vanadium and chromium separation from the vanadium titanomagnetite was also performed using the macroporous weakly basic D314 anion exchange resin [13]. The separation was completed in the pH range of 2.5–6.5 by double adsorption. On the other hand, double adsorption could increase the reagent cost and the operation time results limiting its practical application. To minimize the total cost of vanadium and chromium separation, the pretreatment method was applied [14]. V(V) and Cr(VI) were reduced with  $NaHSO_3$  (pH 1.7); then,  $VO^{2+}$  ions were oxidized by  $H_2O_2$  to the  $H_2V_{10}O_{28}^{4-}$  anions (pH 3.5); on the other hand,  $Cr^{3+}$  ions were not oxidized, and after that, V and Cr were separated by the Dex-V anion exchange resin due to different charge natures.

Based on many examples of vanadium removal and separation by the ion exchange resins of excellent physical and chemical stability (strongly basic anion exchange resins) and regenerative and reuse capabilities (weakly basic anion exchange resins), their adsorption capabilities are strongly affected by pH and co-existing inorganic ions [1]. Therefore, the choice of proper ion exchange resins for vanadium removal from wastewater is precisely dependent on wastewater composition, co-ions and its concentration, and should be individually selected.

The aim of the studies was to determine the efficiency of V(V) ion removal from the model's aqueous solutions and real wastewater (obtained after the digestion of spent catalyst for sulfuric acid production) using ion exchangers of weakly (Purolite A830, abbr.

A830; abbr.—abbreviation), weakly basic/chelating (Purolite S984, abbr. S984), and strongly basic (Lewatit MonoPlus SR7, abbr. SR7; Purolite A400TL, abbr. A400TL; Dowex PSR2, abbr. PSR2; Dowex PSR3, abbr. PSR3) ion exchange resins of different functional groups and microporous Lewatit AF5 (abbr. AF5) without functional groups for comparison. These ion exchangers and the AF5 sorbent adsorption ability toward vanadium have not been described in the literature yet, and the studies fill in the gap developing knowledge about vanadium removal. The optimization of the adsorption process: the adsorbent mass, phase contact time, pH, initial concentration of V(V) ions, and the determination of the maximum adsorption capacities as well as the desorption studies were presented. In this paper, kinetic and equilibrium models were used to describe the vanadium adsorption process and a possible adsorption mechanism was proposed.

## 2. Results

### 2.1. Sorbent Characteristics

The sorbents selected for vanadium removal are macroporous or microporous, including polystyrene, polyacrylic matrices with different functional groups (FG) or a carbonaceous matrix without FG. The physicochemical properties were presented based on the producer data sheets of SR7, A400TL, PSR2, PSR3, A830, S984, and AF5 sorbents as well as from our previous studies [15,16], and they are collected in Table 1.

**Table 1.** Physicochemical properties of SR7, A400TL, PSR2, PSR3, A830, S984, and AF5 sorbents.

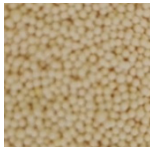
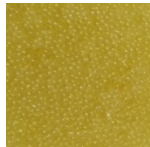





Properties	SR7	A400TL	PSR2	PSR3	A830	S984	AF5
Manufacturer	Lanxess	Lanxess	Dow	Dow	Purolite	Purolite	Lanxess
Type	SBA	SBA	SBA	SBA	WBA	WBA/chelating	sorbent without FG
Matrix	DVB cross-linked polystyrene	DVB cross-linked polystyrene	DVB cross-linked polystyrene	DVB cross-linked polystyrene	DVB cross-linked polyacrylic	DVB cross-linked polyacrylic	carbonaceous
Structure	macroporous	microporous	microporous	macroporous	macroporous	macroporous	microporous
Functional Groups (FG)	quaternary ammonium, type 3	quaternary ammonium, type 1	quaternary ammonium, tri-n-butyl amine		complex amine	polyamine *	without
Size (mm)	0.57–0.67	0.425–0.85	0.3–1.2	0.3–1.2	0.3–1.2	-	0.4–0.8
Max temp. (°C)	80	100 (Cl <sup>-</sup> )60 (OH <sup>-</sup> )	60	60	100 (Cl <sup>-</sup> )40 (OH <sup>-</sup> )	100 (Cl <sup>-</sup> )	300
pH range	0–14	0–14	0–14	0–14	0–9	0–10	0–14
Total capacity (eq/L)	0.6	1.3	0.65	0.6	2.75	2.7	-
Water retention (%)	59–64	48–54	40–48	50–65	47–53	45–55	48–60
Appearance							



Table 1. Cont.

Properties	SR7	A400TL	PSR2	PSR3	A830	S984	AF5
%N	2.58	4.54	2.49	2.25	16.35	18.13	0.02
%C	70.79	59.64	71.38	73.89	46.00	46.95	93.81
%H	6.49	9.76	8.02	10.89	8.39	7.62	1.58
%S	0.26	0.24	1.28	0.06	0.00	0.87	0.91
$S_{BET}$ (m <sup>2</sup> /g)	19.69	4.20	6.32	6.36	9.66	3.80	988.8
$P_s$ (nm)	44.61	2.35	10.08	3.65	48.83	89.36	2.31
$P_v$ (cm <sup>3</sup> /g)	0.220	0.002	0.016	0.006	0.012	0.085	0.572
pH <sub>PZC</sub>	1.48	1.00	1.00	1.03	6.05	9.01	7.09

WBA—the weakly basic anion exchanger; SBA—the strongly basic anion exchanger; DVB—divinylbenzene; \* mixed primary, secondary, and tertiary amines;  $S_{BET}$ —the BET surface area;  $P_s$ —the average pore size;  $P_v$ —the total pore volume.

The chosen examples of SEM images of the sorbents under discussion are presented in Figure 3. All ion exchangers are in the form of round beads of proper size while AF5 is also in the form of beads that are not ideally spherical. This observation and our previous studies also proved the porosity of the ion exchangers. The presence of the functional groups and matrices of the sorbent was proved by using Attenuated Total Reflectance Fourier Transform Infrared Spectroscopy (ATR-FTIR) studies (Figure 4).

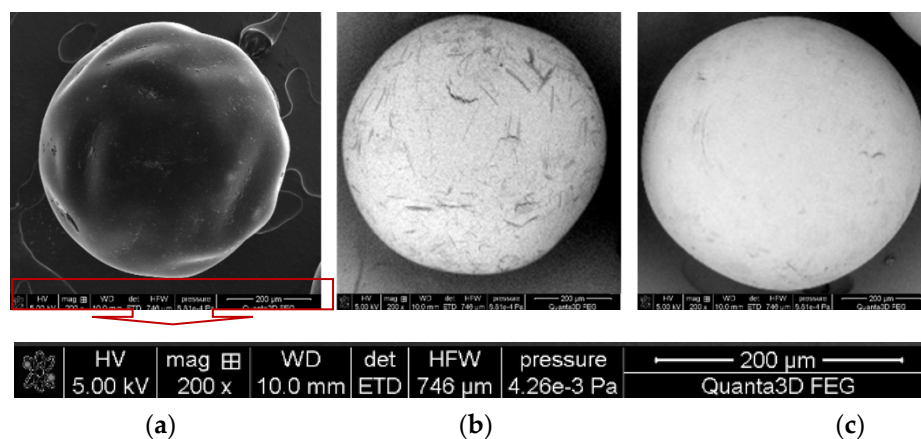


Figure 3. Chosen examples of SEM images of (a) AF5, (b) A830, and (c) SR7 (magn. 200×).

In the ATR-FTIR spectra of ion exchangers before the vanadium(V) sorption process (Figure 4a–c), broad bands of large intensity corresponding to the stretching vibrations of the –OH and =N–H groups were observed at about 3100–3700 cm<sup>−1</sup> [16]. For all anion exchange resins, this peak is observed but the minimum of peak is at wavenumbers 3361 cm<sup>−1</sup> for A400TL, 3351 cm<sup>−1</sup> for SR7, 3352 cm<sup>−1</sup> for PSR2, 3344 cm<sup>−1</sup> for PSR3, 3264 cm<sup>−1</sup> for A830, and 3260 cm<sup>−1</sup> for S984. This wide band indicates the presence of water in the ion exchanger phase [17]. The peaks originating from the ion exchangers matrices (cross-lined polystyrene or cross-linked polyacrylic) were also found in Figure 4a–c. In the wavenumber range of 3000 and 3100 cm<sup>−1</sup> as well as 2800 and 3000 cm<sup>−1</sup>, there were observed narrow bands of high intensity resulting from the aromatic vibrations of the C–H groups as well as the aliphatic symmetric ( $\nu_s$ ) and asymmetric ( $\nu_{as}$ ) C–H stretching vibrations of the –CH<sub>2</sub> group [17–19]. These peaks (Figure 4a,b) are located at 3020 cm<sup>−1</sup>, 2919 cm<sup>−1</sup>, and 2850 cm<sup>−1</sup> for A400TL; at 2936 cm<sup>−1</sup>, 2923 cm<sup>−1</sup>, and 2876 cm<sup>−1</sup> for SR7; and at 2932 cm<sup>−1</sup>, 2925 cm<sup>−1</sup>, and 2872 cm<sup>−1</sup> for PSR2 and PSR3. In the case of WBA resins (Figure 4c), these peaks are less sharp and are located at 3057 cm<sup>−1</sup>, 2930 cm<sup>−1</sup>, and 2847 cm<sup>−1</sup> for A830 and at 3046 cm<sup>−1</sup>, 2923 cm<sup>−1</sup>, and 2867 cm<sup>−1</sup> for S984. Bands in the wavenumber ranging from 1650 to 1400 cm<sup>−1</sup> were also observed (Figure 4a–c). These bands correspond

to carbon–carbon stretching skeletal vibrations inside the benzene ring and C–H groups connected to the aromatic ring [17]. In the wavenumber range of  $1378\text{--}1458\text{ cm}^{-1}$ , bands related to the deformation vibrations in the  $-\text{CH}_2$  group, which are characteristic of the polymer matrix of the ion exchangers, were observed [17,19]. For the SBA resins (A400TL, SR7, PSR3, and PSR2), the characteristic bands located at  $830\text{--}890\text{ cm}^{-1}$ , e.g.,  $887$ ,  $833$ , and  $826\text{ cm}^{-1}$  for A400TL originate from quaternary ammonium functional groups,  $\text{R-N}^+(\text{CH}_3)_3$ , stretching vibrations, and the C–Cl stretching vibration of the  $\text{CH}_2\text{Cl}$  groups, whereas for WBA resins, these bands were not observed [18]. Additionally, for SBA resins, the peaks at  $1460\text{--}1480\text{ cm}^{-1}$  of the C–N vibrations of  $\text{R-N}^+(\text{CH}_3)_3$  appeared [18,20]. In Figure 4d the spectra of Lewatit AF5 are present by the ATR-FTIR method. In these spectra, the peaks for SBA and WBA resins were not observed. There are no peaks that come from the functional groups of the sorbent, and the spectra are different compared to that presented in Figure 4a–c. This sorbent belongs to different types than anion exchange resins and exists in the form of black beads. Moreover, the shape of spectra could be a result of some restriction of ATR-FTIR for samples of high index of refraction (close to that of diamond). The spectrum depends upon the depth of penetration ( $d_p$ ), which in turn depends on other factors, e.g., the ratio of the index of refractions of the sample and crystal. If the sample index is too close to that of the crystal, the ratio of indices is almost 1, the square root term is negative, and there is no ATR effect [21]. The carbonaceous matrix of the Lewatit AF5 was proved by the XRD studies presented in our previous paper [22] and by the %CNHS analysis.

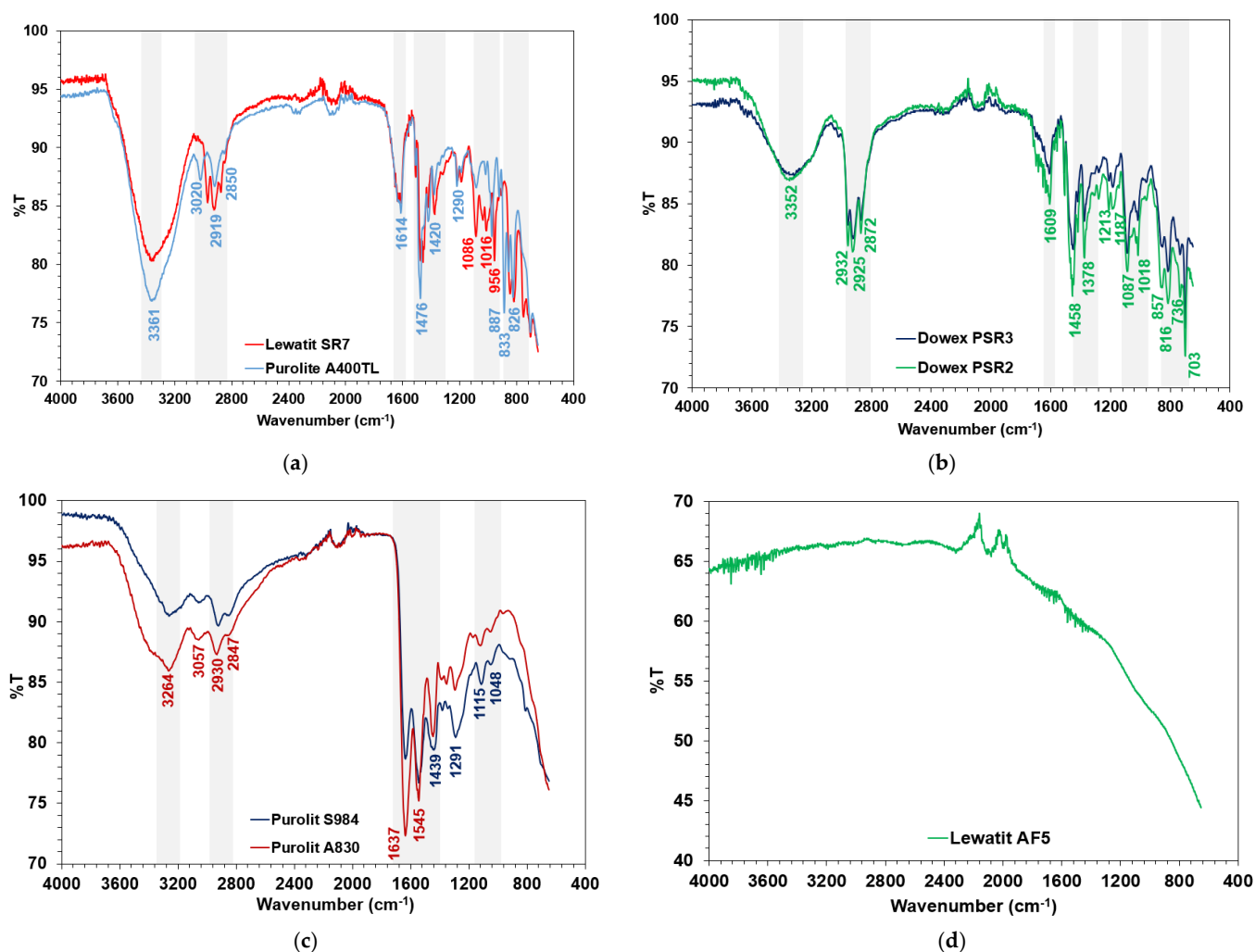


Figure 4. ATR-FTIR spectra: (a,b) SBA resins, (c) WBA resins, and (d) AF5 applied for vanadium (V) removal.

## 2.2. Adsorption Studies—Static and Dynamic Methods

The adsorption studies of vanadium(V) removal were carried out using static and dynamic methods. The adsorption efficiency of SR7, A400TL, PSR2, PSR3, A830, S984, and AF5 sorbents towards V(V) was estimated with the percentage removal (%R) (Equation (1)), the sorption capacity ( $q_e$ ) (Equation (2)), the amount of V(V) adsorbed after time  $t$  ( $q_t$ ) (Equation (3)) values (the static studies), and the weight ( $D_w$ ) (Equation (4)) and bed ( $D_b$ ) (Equation (5)) distribution coefficients as well as the working ion exchange capacity ( $C_w$ ) (Equation (6)) (the column studies) (Table 2).

**Table 2.** Adsorption efficiency determination by static and dynamic studies.

Parameters	Equation	No.
<b>Static method</b>		
percentage removal (%R)	$\%R = \frac{C_0 - C_t}{C_0} \times 100\%$	(1)
sorption capacity ( $q_e$ ) (mg/g)	$q_e = \frac{(C_0 - C_e) \times V}{m}$	(2)
amount of V(V) adsorbed after time $t$ ( $q_t$ ) (mg/g)	$q_t = \frac{(C_0 - C_t) \times V}{m}$	(3)
<b>Dynamic method</b>		
weight distribution coefficient ( $D_w$ )	$D_w = \frac{U'' - U_0 - V_f}{m_j}$	(4)
bed distribution coefficient ( $D_b$ )	$D_b = D_w \times d_z$	(5)
working ion exchange capacity ( $C_w$ ) (g/mL)	$C_w = \frac{U_p \times C_0}{V_j}$	(6)

$C_0, C_e, C_t$ —the initial, equilibrium, and after time  $t$  concentration of V(V) in the water phase (mg/L);  $V$ —the volume of solution;  $m$ —the mass of dry sorbent;  $U'', U_0$ —the eluate volume for  $C/C_0 = 0.5$  (mL) and the dead column volume (2 mL);  $V_f$ —the free volume of the sorbent bed (4 mL);  $m_j$ —the mass of dry sorbent in the column (g);  $d_z$ —the sorbent density (g/mL);  $U_p$ —the volume of eluate to the break through the column (L);  $C_0$  in Equation (6)—the initial V(V) concentration in the solution (g/L);  $V_j$ —the volume of the sorbent in the column.

### 2.2.1. Batch Adsorption—Effect of Adsorbent Doses

The dose of the sorbent is an important parameter affecting the number of sorption sites of the sorbents, their surface areas, and economical costs of adsorption [2]. Studies on the effects of the adsorbent dose ( $0.01$  to  $0.1 \pm 0.0005$  g) on the vanadium(V) adsorption process were carried out at the initial concentration of V(V) ions  $C_0 = 50$  mg/L, temperature  $T$  of 295 K with the agitation speed 170 rpm, the amplitude,  $A = 8$ , and the phase contact time,  $t = 4$  h, according to the batch method described in Section 3.2. The adsorption efficiency results are presented in Figure 5. The plot of the sorbent dose versus the percentage removal (Figure 5a) shows that the %R values increased from 67.9 to 97% for SR7, from 84.8 to 88% for A400TL, from 41.6 to 97.4% for A830, from 36 to 45.5% for PSR2, from 33.2 to 97.7% for PSR3, from 50.3 to 88.2% for S984, and from 0.5 to 19.8% for AF5 with the increase in the sorbent mass from 0.01 to 0.1 g. On the other hand, adsorption capacities decrease with sorbents' mass increase, e.g., from 44.9 to 6.4 mg/L for SR7, from 56 to 5.82 mg/L for A400TL, from 27.5 to 6.4 mg/L for A830, from 23.8 to 3.0 mg/L for PSR2, from 22.0 to 6.4 mg/L for PSR3, and from 33.2 to 5.8 mg/L for S984. In the case of Lewatit AF5,  $q_e$  values slightly increased from 0.4 to 1.7 mg/L and then decreased to 1.3 mg/L. With the sorbent's mass increase, the surface area and number of the active sites increase. At the same initial concentration of V(V) during the sorption, the number of unsaturated adsorption sites increases with increasing sorbent mass. Taking into account the values of %R, the optimal sorbent mass selected for further research is 0.1 g.

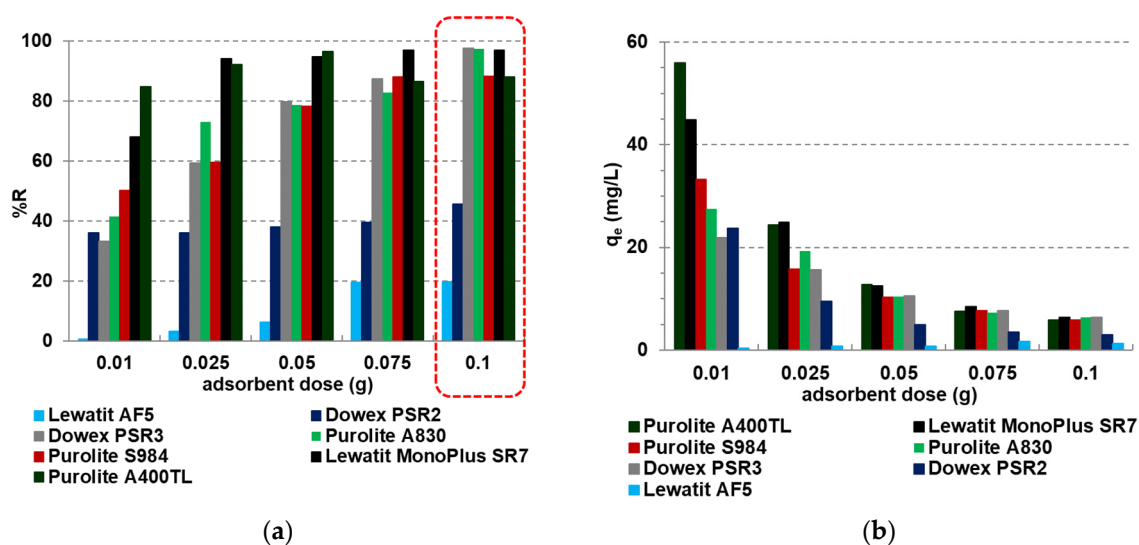


**Figure 5.** Effects of sorbent mass on (a) the percentage removal (%R), (b) sorption capacity ( $q_e$ ) values obtained during the V(V) sorption on the sorbents under discussion.

Generally, on the one hand, the adsorption efficiency increases with the increase in adsorbent dosage; the number of active sites and its availability are greater. However, on the other hand, the adsorption capacity per unit weight of the sorbent decreases with the increase in sorbent doses—the interactions of active sites of the sorbent with the removal contaminants [2,11,17]. For example, the V(V) removal efficiency reached 97.79% for Amberlite IRA743, 95.21% for Lewatit MK51, 84.72% for Purolite S110, and 99.89% for Purolite S108 by increasing the dosage of macroporous ion exchangers (the polystyrene matrix cross-linked with divinylbenzene with the N-methyl-D-glucamine groups) from 0.05 to 0.20 g, but the sorption capacities decreased from 18.70 to 11.36 mg/g for Amberlite IRA743, from 24.53 to 11.06 mg/g for Lewatit MK51, from 19.23 to 9.85 mg/g for Purolite S110, and from 34.86 to 11.61 mg/g for Purolite S108 with the increase in the adsorbent's mass from 0.05 to 0.20 g. In this case, the optimal adsorbent mass was 0.05 g [17]. Similar observations were also made in our previous studies of V(V) removal by Lewatit MonoPlus TP220 and Dowex M4195 of bis-picolylamine functional groups. In that case, the optimal adsorbents mass was also 0.1 g [11]. The increase in the biochar-stabilized nano-zero-valent iron (nZVI/BC) in dose from 0.2 to 1.5 g/L shows that the V(V) removal performance was not satisfactory at doses smaller than 0.5 g/L (removal efficiency 79%), and it increased to 98% with the dose of nZVI/BC, increased to 0.5 g/L, and reached 100% at the dosage above 0.8 g/L. At the same time, the adsorption capacity of V(V) decreased from 48.2 mg/g to 31.4 mg/g. The optimal sorbent dose was selected to be 0.5 g/L [23]. The literature reports that in some cases, the vanadium removal efficiency despite the increasing sorbent dose is unchanged [24] or the increasing adsorbent dose changes the solution's pH; e.g., pH decreases with an increasing dosage of ferric oxyhydroxide, CFH-12 (leaching of impurities), or increases with an increasing dosage of raw zeolite (leaching of hydroxides from the pores due to the alkaline-based synthesis procedure) [24,25].

### 2.2.2. Batch Adsorption—Effects of Solutions pH

Solution pH can influence directly on both the adsorbent properties (surface charge) and vanadium speciation in the aqueous solutions and simultaneously on the vanadium removal efficiency [26]. The surfaces of the adsorbents could be negatively or positively charged when  $\text{pH} > \text{pH}_{\text{pzc}}$  (repulsion between the vanadium anion and the sorbent surface) or  $\text{pH} < \text{pH}_{\text{pzc}}$  (positively charged surface favor adsorption of the vanadium anion). In the aqueous solutions vanadium(V) exists in the form of different soluble species depending on pH and log of the total vanadium concentrations [27–30]. Cationic, neutral and anionic species as well as the other mono- or poly-vanadate ones can be found (Figure 2 in [11],

Figure 6a). At low pH ( $\text{pH} < 3$ ) vanadium exists mostly as the cationic species ( $\text{VO}_2^+$ ) whereas at higher pH values ( $\text{pH} > 3$ ) there exist the anionic species such as the mono-vanadate ones ( $\text{H}_2\text{VO}_4^-$ ,  $\text{HVO}_4^{2-}$ ,  $\text{VO}_4^{3-}$  as the site of protonation is oxygen therefore more precise representation would be  $\text{VO}_2(\text{OH})_2^-$ ,  $\text{VO}_3(\text{OH})_2^{2-}$ ,  $\text{VO}_4^{3-}$ ), the polyvanadate species  $\text{HV}_2\text{O}_7^{3-}$ ,  $\text{V}_2\text{O}_7^{4-}$ ,  $\text{V}_3\text{O}_9^{3-}$ ,  $\text{V}_4\text{O}_{12}^{4-}$ ) and the decavanadate species ( $\text{H}_2\text{V}_{10}\text{O}_{28}^{4-}$ ,  $\text{HV}_{10}\text{O}_{28}^{5-}$ ,  $\text{V}_{10}\text{O}_{28}^{6-}$ ) [27,28,31]. At the low vanadium concentration the monomeric species are observed whereas with the increasing V concentration condensation process occurs [31].

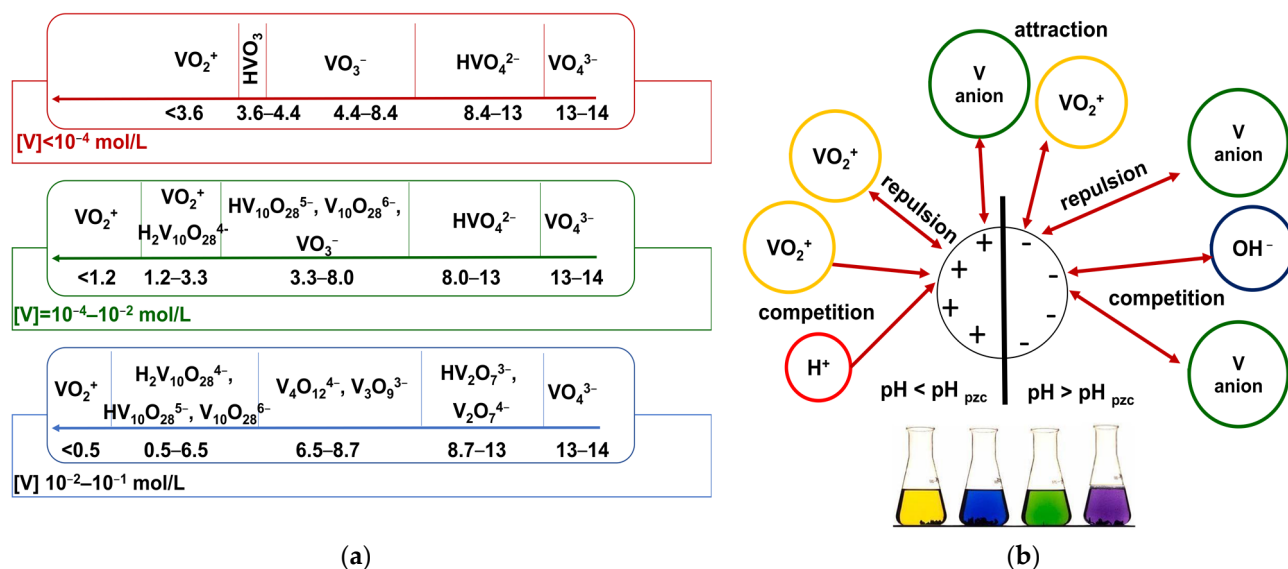


**Figure 6.** Vanadium species (a) and possible interactions with an adsorbent (b) depending on its concentration (a), pH (a,b), and surface charge (b).

The effects of solutions pH (2–10) on the vanadium(V) removal efficiency on the SR7, A400TL, PSR2, PSR3, A830, S984, and AF5 sorbents are presented in Figure 7 (0.1 g,  $C_0 = 50$  mg/L,  $T = 295$  K, 170 rpm,  $A = 8$ ,  $t = 4$  h). As observed, the smallest adsorption capacities were obtained for  $\text{pH} < 3$  as a result of (a) the electrostatic repulsion of main dominant  $\text{VO}_2^+$  species in the solutions of  $\text{pH} < 3$  between vanadium and the positive charges of the sorbent surface and (b) the competition of  $\text{H}^+$  ions with  $\text{VO}_2^+$  for the active site on the adsorbent results in adsorption efficiency reductions [7] (Figure 6b). As it was pointed out by Bello et al., the small sorption capacity of zero-valent iron (ZVI) conjugating with the kaolin clay (Slu-KZVI) sorbent towards vanadium in the solution of  $\text{pH} < 3$  could be also a result of the destruction of the adsorbent structure at a very small pH and the release of adsorbed vanadium into the solution [32].



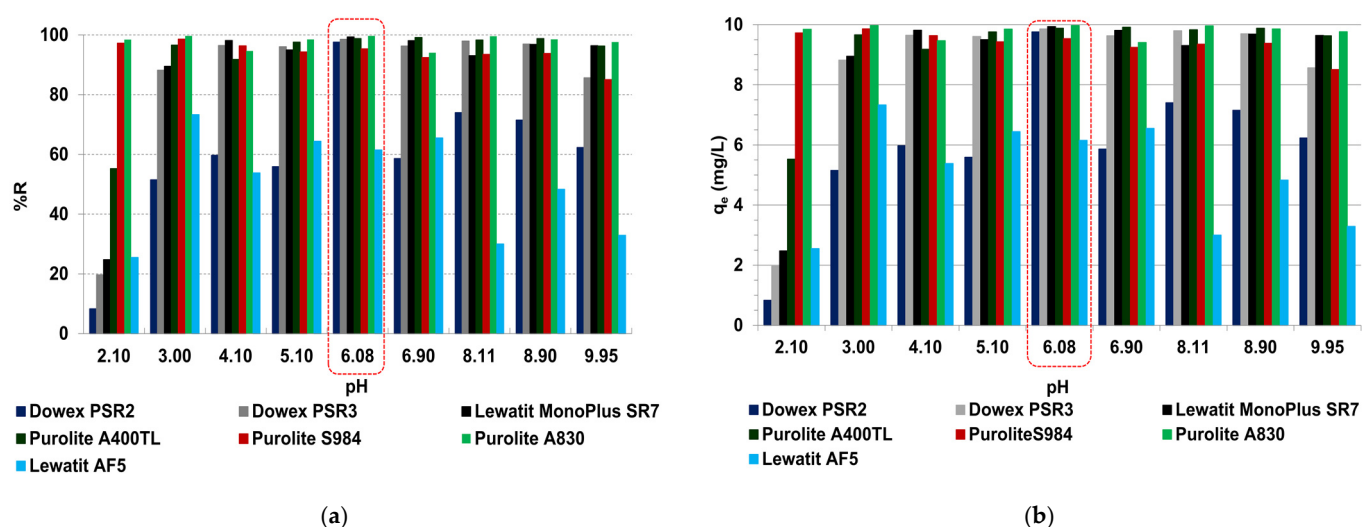
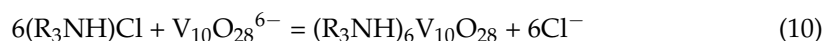
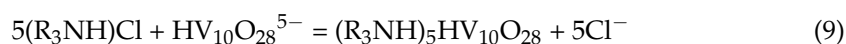
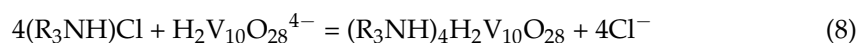


**Figure 7.** Effects of solutions pH on (a) the percentage removal (%R), (b) sorption capacity ( $q_e$ ) values obtained during the V(V) sorption on the sorbents under discussions (50 mg V(V)/L, 4 h, 0.1 g).

Most SR7, A400TL, PSR2, PSR3, A830, S984, and AF5 sorbents exhibit the great sorption capacities at pH 3–9, and the highest values were observed at pH  $\approx$  6; therefore, this pH was chosen in further studies. Moreover, for the WBA resins A830 and S984 (WBA/chelating), the capacities are high in the entire range of examined pH 2–10. In acidic solutions, the functional groups of WBA resin could be protonated [33]. At pH 3–9, vanadium exists in the form of polynuclear anions, e.g.,  $V_2O_6(OH)^{3-}$ ,  $V_2O_7^{4-}$ ,  $V_3O_9^{3-}$ , and  $V_4O_{12}^{4-}$ ; therefore, the interaction of the vanadium anionic species and the anion exchange resins occurs [2]. The possible mechanism of vanadium adsorption could be through the ligand and anion exchange with the functional groups on the adsorbents [9]. The ion exchange reactions of vanadium adsorption on the resin in the  $Cl^-$  form can be expressed as follows.



The electrostatic attractions between the positively charged surface groups of the adsorbent and the anionic vanadium species favour V adsorption [34]. At pH 9, the adsorption capacities decrease as a result of the competition effect between the  $OH^-$  ions and V anions of the adsorption sites (Figure 7) [35]. Additionally, at high pH, vanadium polynuclear species are converted to mononuclear ones; therefore, more adsorption sites are needed for V adsorptions [34]. Similarly to our findings, the literature reports that the maximum adsorption capacities for vanadium were acquired at pH 3–9 [2]. The optimal pH values selected for vanadium adsorptions were pH 11.5 for SBA Amerlite IRA400 (%R = 99.6%) [36], pH 7 for the cation exchanger Amberjet™ 1200 H (%R = 70–75%) [24], pH 7 for anion exchanger Amberjet™ 4200 Cl (%R = 89%) [24], pH 4–7 for the Amberlite IRA-904 modified with tetrakis (p-carboxyphenyl) porphyrin (%R > 80%) [37], etc.

### 2.2.3. Batch Adsorption—Effects of Contact Time

The phase contact time is an important factor affecting both adsorption performance and adsorption economy; therefore, the vanadium adsorption effectiveness was analyzed by also taking into account these factors. The phase contact time was in the range from 1 min to 24 h ( $0.1 \pm 0.0005$  g,  $C_0 = 50, 100, 200$  mg V(V)/L for SR7, A400TL, PSR2, PSR3, A830, S984 or 5, 10, 20, 50, 100 mg/V(V)/L for AF5,  $V = 20$  mL, pH  $\approx$  6, 170 rpm,  $A = 8$ ,

$T = 295$  K). The kinetic curves for different initial concentrations of V(V) ions are presented in Figure 8a–d (chosen examples). In the case of the Lewatit AF5 sorbent without functional groups at an initial vanadium concentration of 100 mg/L, vanadium removal was not observed (Figure 8d); therefore, much smaller initial concentrations at 5, 10, and 20 mg/L were selected. Compared with the other sorbents in the selectivity series, this sorbent takes the last position and shows the smallest adsorption capacities at 0.4 mg/g for  $C_0 = 5$  mg/L, 0.7 mg/g for  $C_0 = 10$  mg/L, 1.3 mg/g for  $C_0 = 20$  mg/L, and 1.6 mg/g for  $C_0 = 50$  mg/L (Figure 8d).

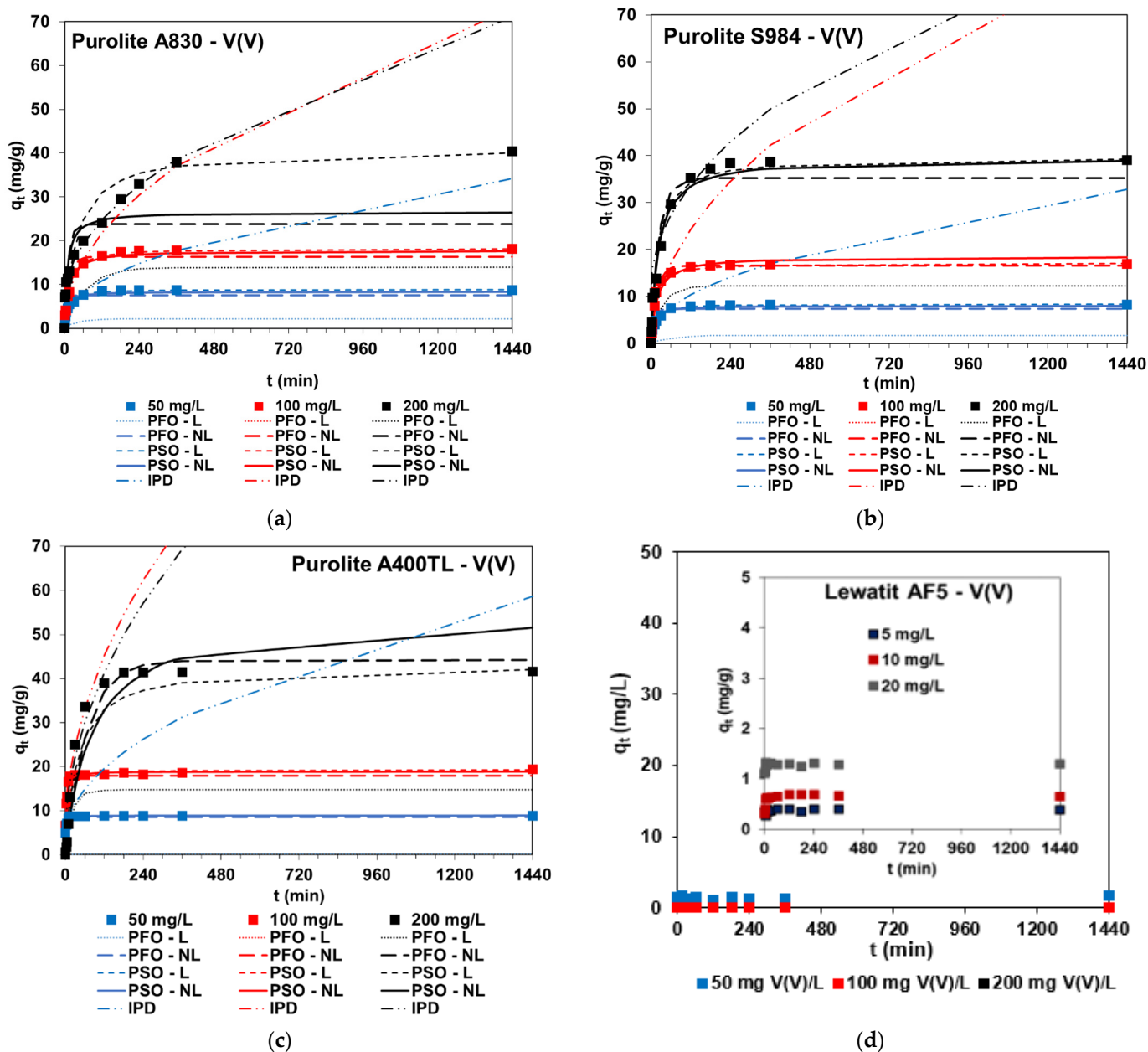


Figure 8. Effects of phase contact time and initial concentration on the amount of vanadium adsorbed on (a) A830, (b) S984, (c) A400TL, and (d) AF5.

Based on the kinetic studies, the following can be concluded:

- Vanadium kinetic plots usually included two stages: (1) fast adsorption due to great accessibility of free adsorption sites and (2) slower adsorption stage and reaching

equilibrium—the remaining adsorption site's availability is more difficult [17]. In the case of 200 mg V(V)/L concentrations, three stages can usually be distinguished.

- The amount of V(V) ions adsorbed increase with the increasing phase contact time, e.g.,  $q_t = 5 \text{ mg/g}$  ( $t = 1 \text{ min}$ ) and  $q_t = 8.7 \text{ mg/g}$  ( $t = 30 \text{ min}$ ) for  $C_0 = 50 \text{ mg/L}$  and A400TL, but the shape of the kinetic curves and their “steepness” depend on the initial concentrations of V(V) ions present in the solution.
- The adsorption capacities usually increase with increasing initial concentrations, e.g.,  $q_e = 8.8 \text{ mg/g}$  ( $C_0 = 50 \text{ mg/L}$ ),  $q_e = 19.3 \text{ mg/g}$  ( $C_0 = 100 \text{ mg/L}$ ), and  $q_e = 40.1 \text{ mg/g}$  ( $C_0 = 200 \text{ mg/L}$ ) for A400TL.
- The time required for equilibrium establishment depends on the initial vanadium concentration: longer times are needed for the equilibrium establishment for systems containing 100 and 200 mg V(V)/L compared to 50 mg V(V)/L. Comparing the equilibrium time for vanadium removal ( $t_{eq}$ ) by various sorbents, e.g., SBA resin Amberlite IRA-400 ( $t_{eq} = 5 \text{ min}$ ) [6], SBA resin Amberlite IRA-400 ( $t_{eq} = 60 \text{ min}$ ) [5], SBA resin D296 ( $t_{eq} = 12 \text{ h}$ ) [8], WBA resin 201\*7 ( $t_{eq} = 20 \text{ min}$ ) [38], WBA resin ZGA414 ( $t_{eq} = 8 \text{ min}$ ) [10], nano-hydrous zirconium oxide-modified anion exchange resin, ( $t_{eq} = 2 \text{ h}$ ) [34], N235 impregnated resin (NIRs) ( $t_{eq} = 10 \text{ h}$ ), N235-TBS-impregnated resin (N-TIRs) ( $t_{eq} = 6 \text{ h}$ ) [39], di-(2-ethylhexyl) phosphoric acid (D2EHPA)-Tributyl phosphate (TBP)-impregnated resin ( $t_{eq} = 36 \text{ h}$ ) [40] and that presented in the review paper in Table 2 [2] and taking into account this paper,  $t_{eq}$  is highly variable, ranging from a few minutes to 48 h.
- With the higher V(V) concentration, the percentage removal of vanadium is smaller, e.g., 99.9%, 98.6%, 94.4% for 50, 100, and 200 mg V(V)/L, and A400TL or 38.9%, 33.0%, 32.7%, and 18.5% for 5, 10, 20, and 50 mg V(V)/L, and AF5, respectively.

From the practical point of view and considering the applicability of sorbents in industry, the obtained experimental kinetic data were modeled with commonly used kinetic equations such as the pseudo-first order kinetic equation (PFO), the pseudo-second order kinetic equation (PSO) as well as the intraparticle diffusion (IPD) to describe the V(V) adsorption process:

PFO: non-linear (Equation (11)), linear (Equation (12)):

$$q_t = q_e \left(1 - e^{-k_1 t}\right) \quad (11)$$

$$\log(q_e - q_t) = \log q_e - \frac{k_1}{2.303} t \quad (12)$$

where  $k_1 = -2.303 \times \text{slope}$ ,  $q_e = 10^{\text{intercept}}$ ,  $q_e$  and  $q_t$  (mg/g) are the amounts of V(V) sorbed at the equilibrium and at any time  $t$ ,  $k_1$  (1/min) includes the rate constants determined from the PFO equation, and  $t$  denotes the contact time [41]:

PSO: non-linear (Equation (13)), linear (Equation (14)):

$$q_t = \frac{q_e^2 k_2 t}{q_e k_2 t + 1} \quad (13)$$

$$\frac{t}{q_t} = \frac{1}{k_2 q_e^2} + \frac{1}{q_e} t \quad (14)$$

where  $k_2$  (g/mg min) denotes the rate constants determined from the PSO equation,  $k_2 = \text{slope}^2 / \text{intercept}$ ,  $q_e = 1 / \text{slope}$ ,  $h$  denotes the initial sorption rate, and  $h = k_2 q_e^2$  [42]:

IPD: linear (Equation (15)):

$$q_t = k_i t^{1/2} + C \quad (15)$$

where  $k_i$  (mg/g min<sup>0.5</sup>) denotes the intraparticle diffusion rate constant,  $k_i = \text{slope}$ ,  $C$  denotes the Weber–Morris diffusion constant, and  $C = \text{intercept}$  [43].

The obtained kinetic parameters using the PFO, PSO, and IPD models with linear (L) and non-linear (NL) regressions are presented in Table 3. Due to the kinetic curve's shape

and experimental points position (AF5) and smaller than 10 mg/g sorption capacity for 50 and 100 mg V(V)/L (SR7, PSR2, and PSR3), the kinetic parameters were not calculated (AF5) or calculated but not presented in Table 3 (50, 100 mg/L for SR7, PSR2, PSR3).

**Table 3.** Comparison of kinetic parameters obtained during the V(V) adsorption.

Parameters		A830			S984			A400TL			SR7	PSR2	PSR3
$C_0(\text{mg/L})$		50	100	200	50	100	200	50	100	200	200	200	200
$q_{e, exp}$		8.77	18.09	40.38	8.30	16.95	39.10	8.82	19.34	41.54	40.52	38.88	23.92
PFO-L	$q_{e, cal}$	4.88	10.35	32.04	3.94	8.46	28.27	0.62	3.44	33.91	10.30	14.23	17.04
	$k_1$	0.022	0.012	0.007	0.013	0.014	0.013	0.019	0.005	0.021	0.025	0.007	0.004
	$R^2$	0.957	0.906	0.985	0.906	0.896	0.959	0.710	0.439	0.954	0.959	0.904	0.909
PFO-NL	$q_{e, cal}$	7.56	16.32	23.83	7.40	16.54	35.18	8.45	17.90	44.18	37.95	30.03	12.85
	$k_1$	0.137	0.066	0.088	0.104	0.058	0.043	0.772	0.384	0.015	0.384	0.561	0.147
	$R^2$	0.865	0.950	0.645	0.886	0.991	0.962	0.798	0.938	0.960	0.853	0.429	0.610
	$R^2_{adj}$	0.834	0.939	0.566	0.861	0.989	0.953	0.753	0.924	0.951	0.821	0.302	0.524
	MPSD	0.379	0.638	1.359	0.645	0.062	0.411	0.067	0.061	0.398	0.185	0.455	0.695
	$\chi^2$	1.79	2.93	24.79	2.06	0.39	4.58	13.40	29.47	19.89	4.22	12.43	11.14
	SSE	11.36	21.23	690.39	8.45	3.94	92.82	92.11	392.62	237.27	106.95	367.31	212.68
PSO-L	$q_{e, cal}$	8.83	18.26	41.22	8.35	17.11	39.74	8.82	19.35	43.10	40.59	39.02	24.25
	$k_2$	0.017	0.004	0.001	0.015	0.006	0.001	0.178	0.010	0.001	0.014	0.003	0.001
	$R^2$	1.000	1.000	0.996	1.000	1.000	1.000	1.000	1.000	0.996	1.000	1.000	0.991
	$h$	1.32	1.49	1.04	1.07	1.62	2.10	13.87	3.76	1.16	22.98	4.22	0.49
PSO-NL	$q_{e, cal}$	8.33	17.77	26.63	7.98	18.53	39.51	8.83	18.88	54.40	39.79	32.74	14.82
	$k_2$	0.020	0.004	0.004	0.017	0.003	0.001	0.138	0.028	0.000	0.015	0.022	0.010
	MPSD	0.1245	0.4581	0.9113	0.416	0.139	0.225	0.009	0.009	0.603	0.058	0.226	0.410
	$R^2$	0.963	0.980	0.768	0.947	0.972	0.988	0.973	0.984	0.909	0.960	0.727	0.765
	$R^2_{adj}$	0.952	0.975	0.702	0.936	0.966	0.985	0.967	0.981	0.888	0.951	0.666	0.712
	$\chi^2$	0.55	1.75	16.73	3.78	8.33	12.15	0.06	0.15	12.86	1.25	5.91	6.78
IPD	SSE	3.31	8.72	471.92	11.37	74.72	184.29	0.45	2.53	387.61	28.22	167.68	131.14
	$q_{e, cal}$	34.22	73.36	71.14	32.79	84.76	88.06	58.62	147.0	135.4	50.25	49.01	32.45
	$k_i$	0.87	1.91	1.72	0.83	2.24	2.01	1.44	3.76	3.48	0.39	0.54	0.69
	$R^2$	0.943	0.967	0.995	0.979	0.908	0.913	0.960	0.950	0.901	0.860	0.859	0.948
	$R^2_{adj}$	0.914	0.950	0.993	0.968	0.862	0.738	0.881	0.900	0.703	0.581	0.577	0.922

$q_{e, exp}$  (mg/g),  $q_{e, cal}$  (mg/g),  $k_1$  (1/min),  $k_2$  (g/mg min),  $k_i$  (mg/g min<sup>0.5</sup>).

The Lagergren equation did not find applicability for the description of the V(V) adsorption kinetics on the sorbents under discussion due to the small values of the determination coefficients  $R^2$  being in the range of 0.439–0.985 (L) and  $\leq 0.991$  (NL). In addition, the calculated equilibrium capacities were much smaller than those determined experimentally (Figure 8). Moreover, the graph  $\log(q_e - q_t)$  vs.  $t$  was not linear (e.g., Figure 9a).

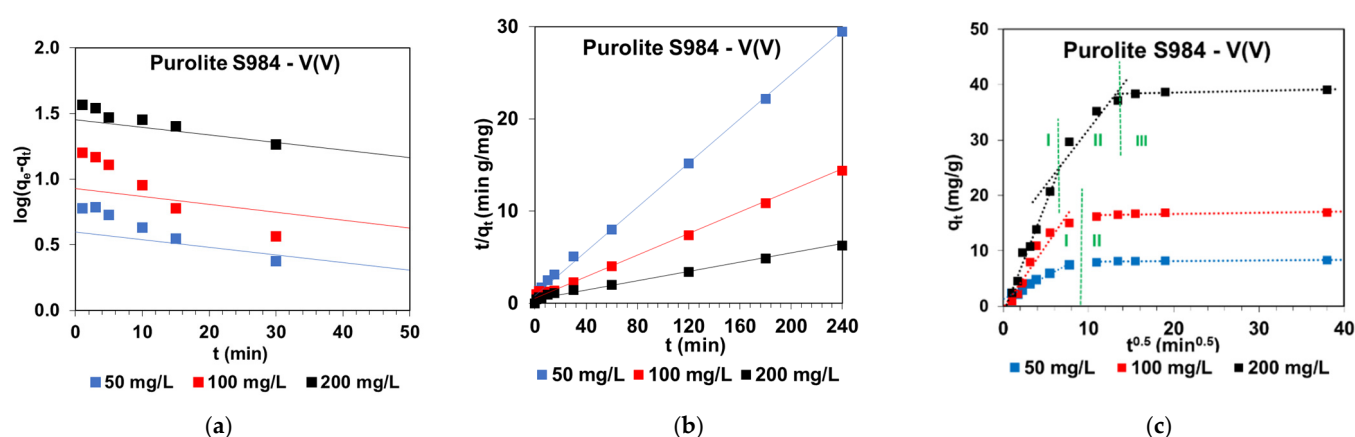


**Figure 9.** Examples of (a) PFO, (b) PSO, and (c) IPD plots obtained during the V(V) adsorption on Purolite S984.

Figure 9b shows the example of the linearized form of the PSO kinetic dependence for V(V) adsorption from the solutions of different initial concentrations on Purolite S984 and the plot  $t/q_t$  vs.  $t$  shows the linear relationship. Moreover, based on the data presented in Table 3 and Figure 8, it can be concluded that due to large values of the determination coefficient for PSO-NL or very large values for PSO-L and great agreement between the adsorption capacity determined experimentally and calculated from PSO-L, the PSO-L model received the best fit to the experimental data for SR7, A400TL, PSR2, PSR3, A830, and S984 sorbents.

The IPD plots obtained for the SR7, A400TL, PSR2, PSR3, A830, and S984 sorbents show the applicability of the intraparticle diffusion model in the V(V) adsorption if the plot of  $q_t$  vs.  $t^{1/2}$  provide a straight line and passes through the origin. If these factors are fulfilled, the intraparticle diffusion is the only rate-controlling step of the vanadium adsorption process; otherwise, it is not the only rate limiting step. The obtained IPD plots (e.g., Figure 9c) illustrate multi-linearity. The adsorption data can be fitted with two (A830) or three (SR7, A400TL, PSR2, PSR3, and S984) straight lines. The proper parts of the IPD graph correspond to the diffusion effects by the boundary layer or intraparticle diffusion (diffusion into the polymer network). As it was found, the IPD plots do not pass through the origin in all cases, indicating that apart from the intraparticle diffusion, other factors also have an influence on the adsorption rate. Similar observations were also made by other research studies during the V(V) adsorption on various sorbents, e.g., Burdzy et al. [17], Stanisz et al. [44], and Kajjumba et al. [45] (please see also column kinetic studies in Table 4).

**Table 4.** Kinetic and equilibrium studies for vanadium on ion exchangers and biochar—comparison.

Adsorbent	Kinetic Studies	Isotherm Studies	Ref.
	* linear, ** non-linear regression		
Amberlite® IRA-400	<p><math>W = 10</math> g; <math>V = 150</math> mL; 150 rpm; <math>t = 1</math>–30 min; <math>T = 20</math> °C</p> <p>Post-closure effluent: <math>C_0 = 5.3</math> mg/L; pH 11.5</p> <p>Op. BRDA leachate: <math>C_0 = 4.7</math> mg/L; pH 13.3</p> <p>* PFO</p> <p>Post-closure effluent: <math>k_1 = 1.181</math> 1/min; <math>R^2 = 0.977</math></p> <p>Op. BRDA leachate: <math>k_1 = 0.545</math> 1/min; <math>R^2 = 0.985</math></p>	<p><math>V = 20</math> mL; <math>C_0 = 1</math>–50 g/L; 150 rpm; <math>t = 30</math> min; <math>T = 20</math> °C</p> <p>Langmuir (L), Freundlich (F)</p> <p>Post-closure effluent: pH 11.5</p> <p>L: <math>q_{max} = 1.135</math> mg/g; <math>b = 3.218</math> L/mg; <math>R^2 = 0.859</math>,</p> <p>F: <math>k_F = 0.547</math>; <math>n = 2.383</math>; <math>R^2 = 0.999</math>,</p> <p>Op. BRDA leachate: pH 13.3</p> <p>L: <math>q_{max} = 9.759</math> mg/g; <math>b = 0.060</math> L/mg; <math>R^2 = 0.919</math>,</p> <p>F: <math>k_F = 0.285</math>; <math>n = 1.050</math>; <math>R^2 = 0.993</math></p>	[36]



Table 4. Cont.

Adsorbent	Kinetic Studies	Isotherm Studies	Ref.
Lewatit MonoPlus TP220; Dowex M4195	<p><math>W = 0.1 \pm 0.0005</math> g; <math>C_0 = 50; 100; 200</math> mg V(V)/L; <math>V = 20</math> mL; pH 4; 170 rpm, <math>A = 8</math>; <math>T = 295</math> K, <math>t = 1</math> min–24 h</p> <p>*, ** PFO, <b>PSO</b>, IPD</p> <p><math>C_0 = 50</math> mg/L, * PSO: <math>q_{e\text{ cal}} = 7.68</math> mg/g; <math>k_2 = 0.018</math> g/mg min; <math>R^2 = 0.998</math>, TP220</p> <p><math>C_0 = 50</math> mg/L, * PSO: <math>q_{e\text{ cal}} = 9.54</math> mg/g; <math>k_2 = 0.021</math> g/mg min; <math>R^2 = 0.999</math>, M4195</p>	<p><math>W = 0.1 \pm 0.0005</math> g; <math>C_0 = 50\text{--}2000</math> mg V(V)/L; <math>V = 20</math> mL; pH 4; 170 rpm, <math>A = 8</math>; <math>T = 295</math> K; <math>t = 24</math> h</p> <p>*, ** <b>Langmuir (L)</b>, Freundlich (F), Temkin (T), Dubinin-Radushkevich (D-R)</p> <p>* L: <math>q_{\text{max}} = 247.8</math> mg/g;</p> <p><math>k_L = 0.014</math> L/mg; <math>R^2 = 0.963</math>, TP220;</p> <p>* L: <math>q_{\text{max}} = 208.8</math> mg/g;</p> <p><math>k_L = 0.037</math> L/mg; <math>R^2 = 0.998</math>, M4195</p> <p>**F and L, TP220; ** L and T, M4195</p>	[11]
Amberlite IRA743; Lewatit MK51; Purolite S110; Purolite S108	<p>1 g/L; <math>C_0 = 10\text{--}100</math> mg V(V)/L; pH 5; 180 rpm, <math>A = 7</math>; <math>T = 293</math> K, <math>t = 1\text{--}240</math> min</p> <p>** PFO, <b>PSO</b>, IPD, Boyd</p> <p><math>C_0 = 50</math> mg/L:</p> <p>** PSO: <math>q_{e\text{ cal}} = 31.28</math> mg/g; <math>k_2 = 0.0017</math> g/mg min; <math>R^2 = 0.978</math>, IRA473</p> <p>** PSO: <math>q_{e\text{ cal}} = 32.35</math> mg/g; <math>k_2 = 0.0015</math> g/mg min; <math>R^2 = 0.992</math>, MK51</p> <p>** PSO: <math>q_{e\text{ cal}} = 39.18</math> mg/g; <math>k_2 = 0.0014</math> g/mg min; <math>R^2 = 0.988</math>, S110</p> <p>** PSO: <math>q_{e\text{ cal}} = 41.06</math> mg/g; <math>k_2 = 0.0021</math> g/mg min; <math>R^2 = 0.994</math>, S108</p> <p>** PFO <math>R^2 = 0.882\text{--}0.999</math>; IPD <math>R^2 = 0.933\text{--}0.993</math>, Boyd <math>0.947\text{--}0.998</math> for all resin and concentration</p>	<p>1 g/L; <math>C_0 = 10\text{--}150</math> mg V(V)/L; pH 5; <math>T = 293, 313, 333</math> K, <math>t = 240</math> min</p> <p>** <b>Langmuir (L)</b>, Freundlich (F), Temkin (T) at 333 K:</p> <p>** L: <math>q_{\text{max}} = 68.27</math> mg/g;</p> <p><math>k_L = 0.122</math> L/mg; <math>R^2 = 0.940</math>, IRA473;</p> <p>** L: <math>q_{\text{max}} = 72.51</math> mg/g;</p> <p><math>k_L = 0.150</math> L/mg; <math>R^2 = 0.975</math>, MK51;</p> <p>** L: <math>q_{\text{max}} = 66.42</math> mg/g;</p> <p><math>k_L = 0.277</math> L/mg; <math>R^2 = 0.989</math>, S110;</p> <p>** L: <math>q_{\text{max}} = 77.03</math> mg/g;</p> <p><math>k_L = 0.416</math> L/mg; <math>R^2 = 0.992</math>, S108;</p> <p>at 293, 313, 333 K:</p> <p>L: <math>R^2 = 0.992\text{--}0.997</math>; F: <math>R^2 = 0.958\text{--}0.998</math>;</p> <p>T: <math>R^2 = 0.802\text{--}0.996</math></p>	[17]
Tulsion A-62	<p><math>W = 0.1</math> g; <math>V = 40</math> mL; 160 rpm, <math>t = 10\text{--}200</math> min</p> <p>%R = 70% (15 min), %R = 97.5% (180 min)</p> <p>no kinetic model was used</p>	<p>* <b>Langmuir (L)</b>, Freundlich (F)</p> <p>L: <math>q_{\text{max}} = 36.9</math> mg/g; <math>k_L = 0.585</math> l/mol; <math>R^2 = 0.964</math>;</p> <p>F: <math>k_F = 15.33</math> mg/g; <math>n = 3.2</math> L/g; <math>R^2 = 0.980</math></p>	[46]
biochars BC2	<p><math>W = 0.5</math> g; <math>C_0 = 10\text{--}50</math> mg V(V)/L; <math>V = 20</math> mL; pH 3; <math>t = 5\text{--}360</math> min</p> <p>* PFO, <b>PSO</b>, IPD</p> <p><math>C_0 = 50</math> mg/L: *PSO: <math>q_{e\text{ cal}} = 0.83</math> mg/g; <math>k_2 = 0.07</math> g/mg min; <math>R^2 = 0.999</math></p> <p><math>C_0 = 10\text{--}50</math> mg/L: *PFO <math>R^2 = 0.912\text{--}0.990</math>; IPD <math>R^2 = 0.816\text{--}0.997</math></p>	<p><math>W = 0.5</math> g; <math>C_0 = 5\text{--}150</math> mg V(V)/L; <math>V = 20</math> mL; pH 3; <math>t = 300</math> min, <math>T = 298</math> K</p> <p>* Langmuir (L), Freundlich (F), Temkin (T), Dubinin-Radushkevich (D-R)</p> <p>* L: <math>q_{\text{max}} = 0.52</math> mg/g; <math>k_L = 0.05</math> L/mg; <math>R^2 = 0.974</math></p> <p>* F: <math>k_F = 0.06</math> mg/g; <math>n = 1.96</math> L/g; <math>R^2 = 0.998</math></p> <p>* T: <math>k_T = 0.82</math> L/g; <math>b_T = 21.62</math> kJ/mol; <math>R^2 = 0.952</math></p> <p>* D-R: <math>q_m = 0.31 \times 10^{-4}</math> mol/g; <math>K_{DR} = 4.7 \times 10^{-3}</math> mol<sup>2</sup>/kJ<sup>2</sup>; <math>R^2 = 0.993</math></p>	[4]

Table 4. Cont.

Adsorbent	Kinetic Studies	Isotherm Studies	Ref.
Purolite A830, Purolite S984, Purolite A400TL, Lewatit MonoPlus SR7, Dowex PSR2, Dowex PSR3, Lewatit AF5	$W = 0.1 \pm 0.0005$ g; $C_0 = 50; 100; 200$ mg $V(V)/L; V = 20$ mL; pH 6; 170 rpm, $A = 8$ ; $T = 295$ K, $t = 1$ min–24 h *, ** PFO, <b>PSO</b> , IPD $C_0 = 50$ mg/L: * PSO: $q_{e\text{ cal}} = 8.83$ mg/g; $k_2 = 0.017$ g/mg min; $R^2 = 1.000$ , A830; * PSO: $q_{e\text{ cal}} = 8.35$ mg/g; $k_2 = 0.015$ g/mg min; $R^2 = 1.000$ , S984; * PSO: $q_{e\text{ cal}} = 8.82$ mg/g; $k_2 = 0.178$ g/mg min; $R^2 = 1.000$ , A400TL; * PSO: $q_{e\text{ cal}} = 8.79$ mg/g; $k_2 = 0.055$ g/mg min; $R^2 = 1.000$ , SR7; * PSO: $q_{e\text{ cal}} = 8.02$ mg/g; $k_2 = 0.005$ g/mg min; $R^2 = 0.997$ , PSR2; * PSO: $q_{e\text{ cal}} = 8.77$ mg/g; $k_2 = 0.039$ g/mg min; $R^2 = 1.000$ , PSR3; AF5-no kinetic model was used	$W = 0.1 \pm 0.0005$ g; $C_0 = 50; 100; 200$ mg $V(V)/L; V = 20$ mL; pH 6; 170 rpm, $A = 8$ ; $T = 295$ K, $t = 24$ h *, ** <b>Langmuir (L)</b> , <b>Freundlich (F)</b> , <b>Temkin (T)</b> , Dubinin-Radushkevich (D-R) * L: $q_{max} = 204.1$ mg/g; $k_L = 0.098$ L/mg; $R^2 = 1.000$ , A830 * L: $q_{max} = 256.62$ mg/g; $k_L = 0.008$ L/mg; $R^2 = 0.927$ , S984; * L: $q_{max} = 204.27$ mg/g; $k_L = 0.0049$ L/mg; $R^2 = 0.999$ , A400TL; * L: $q_{max} = 39.49$ mg/g; $k_L = 0.045$ L/mg; $R^2 = 0.959$ , SR7; * L: $q_{max} = 40.42$ mg/g; $k_L = 0.024$ L/mg; $R^2 = 0.940$ , PSR2; * L: $q_{max} = 39.57$ mg/g; $k_L = 0.31$ L/mg; $R^2 = 0.955$ , PSR3; * F: $k_F = 2.00$ mg $^{1-1/n}$ L $^{1/n}$ /g; $1/n = 0.63$ ; $R^2 = 0.972$ , AF5	This paper

Op. BRDA leachate—operating bauxite residue disposal areas leachate; **bold**—the best fit; BC2—wet distiller grains.

### 2.3. Equilibrium Studies

The experimental data for vanadium adsorption on the S984, A830, A400TL, SR7, PSR2, PSR3, and AF5 sorbents were fitted with the Langmuir, Freundlich, Temkin, and Dubinin–Radushkevich adsorption isotherms (description of isotherms are included in Table 5). The Langmuir isotherm described sorption on the homogenous surface with a finite, limited number of adsorption sites and constant energy without interactions between the sorbed molecules [47]. The Freundlich adsorption isotherm describes the multilayer adsorption on the heterogeneous adsorbent surface (non-ideal adsorption) [36,48]. The sorption centers with the highest sorption energy will be saturated first, and then the centers with increasingly smaller energies are saturated. Due to possible interactions between the adsorbed molecules, the variation of adsorption heat may proceed [49]. The Temkin isotherm model describes the adsorption on a heterogeneous solid and takes into account adsorbate–adsorbent interactions. This model assumes that the heat of adsorption of all molecules in the layer decreases linearly, and the adsorption is characterized by the uniform distribution of binding energy [49,50]. The Dubinin–Radushkevich isotherm model is often used to estimate the free energy of adsorption, which could indicate the physical or chemical adsorption mechanism depending on its values. When  $E$  is in the range from 1 to 8 kJ/mol, the adsorption is a result of physical interactions, while an  $E$  between 8 and 16 kJ/mol indicates the ion exchange, and  $E > 16$  kJ/mol suggests chemical adsorptions [49,51].

**Table 5.** Characterization of the isotherm models and the parameters obtained for the V(V) ions sorption on the S984, A830, A400TL, SR7, PSR2, PSR3, and AF5 sorbents.

Isotherm	Non-linear Forms	Equation	Linear Forms	Equation				
Langmuir	$q_e = \frac{k_L Q_0 C_e}{1 + C_e k_L}$	(16)	$\frac{C_e}{q_e} = \frac{1}{Q_0 k_L} + \frac{C_e}{Q_0}$	(17)				
Freundlich	$q_e = k_F C_e^{1/n}$	(18)	$\log q_e = \log k_F + \frac{1}{n} \log C_e$	(19)				
Temkin	$q_e = \frac{RT}{b_T} \ln A C_e$	(20)	$q_e = \left(\frac{RT}{b_T}\right) \ln A + \left(\frac{RT}{b_T}\right) \ln C_e$	(21)				
Dubinin-Radushkevich	$q_e = q_m e^{k_{DR} \epsilon^2}$	(22)	$\ln q_e = \ln q_m - k_{DR} \epsilon^2$	(25)				
	$\epsilon = RT \ln \left[ 1 + \frac{1}{C_e} \right]$	(23)						
	$E = \frac{1}{\sqrt{2k_{DR}}}$	(24)						
Isotherm Parameters								
Model	Parameters	S984	A830	A400TL	SR7	PSR2	PSR3	AF5
Langmuir	$Q_{e, exp.}$ (mg/g)	221.4	202.00	200.4	30.80	29.28	29.12	27.76
	$Q_0$ (mg/g)	256.62	204.10	204.27	39.49	40.42	39.57	37.98
	$k_L$ (L/mg)	0.008	0.098	0.049	0.045	0.024	0.031	0.035
	$R^2$	0.927	1.000	0.999	0.959	0.940	0.955	0.772
Freundlich	$k_F$ (mg <sup>1-1/n</sup> L <sup>1/n</sup> /g)	5.58	24.19	19.87	1.84	1.13	1.37	2.00
	$1/n$	0.613	0.377	0.395	0.722	0.766	0.745	0.630
	$R^2$	0.691	0.820	0.769	0.963	0.942	0.962	0.972
Temkin	$b_T$ (J/g/mol mg)	52.40	87.12	82.78	386.72	394.73	397.73	537.26
	$A$ (L/mg)	0.170	2.730	1.466	1.198	0.668	0.847	1.806
	$R^2$	0.904	0.947	0.960	0.897	0.954	0.924	0.793
Dubinin-Radushkevich	$q_m$ (mg/g)	159.50	118.45	136.78	15.99	14.39	13.24	10.70
	$k_{DR}$ (mol <sup>2</sup> J <sup>2</sup> )	$6.1 \times 10^{-5}$	$3.76 \times 10^{-7}$	$1.57 \times 10^{-6}$	$4.40 \times 10^{-7}$	$11.3 \times 10^{-7}$	$5.16 \times 10^{-7}$	$1.31 \times 10^{-7}$
	$E$ (kJ/mol)	0.091	1.154	0.565	1.068	0.665	0.985	1.957
	$R^2$	0.921	0.694	0.774	0.747	0.736	0.596	0.513

$q_e$  (mg/g)—the amount of V(V) ions sorbed per unit mass of sorbent;  $C_e$  (mg/L)—the equilibrium concentration of solution;  $Q_0$  (mg/g)—the monolayer adsorption capacity;  $k_L$  (L/mg)—the Langmuir constant (related to the free energy of adsorption);  $k_F$  (mg<sup>1-1/n</sup> L<sup>1/n</sup>/g) and  $1/n$ —the Freundlich constants connected with the adsorption capacity of the adsorbent and the surface heterogeneity;  $R$  (8.314 J/mol K)—the gas constant;  $T$  (K)—the temperature;  $A$  (L/g) and  $b_T$  (J/mol)—the Temkin constants;  $q_m$  (mg/g)—the maximum adsorption capacity;  $k_{DR}$  (mol<sup>2</sup> J<sup>2</sup>)—the constant related to the adsorption energy;  $\epsilon$  (J/mol)—the adsorption potential;  $E$  (J/mol)—the mean free energy for the V(V) ions removal from adsorption site to the infinity.

Characteristic parameters of the obtained Langmuir, Freundlich, Temkin, and Dubinin–Radushkevich isotherm models by linear regression are presented in Table 5 (obtained by the linear regression), whereas the selected examples of fitting plots (linear—L; non-linear—NL regression) are depicted in Figure 10.

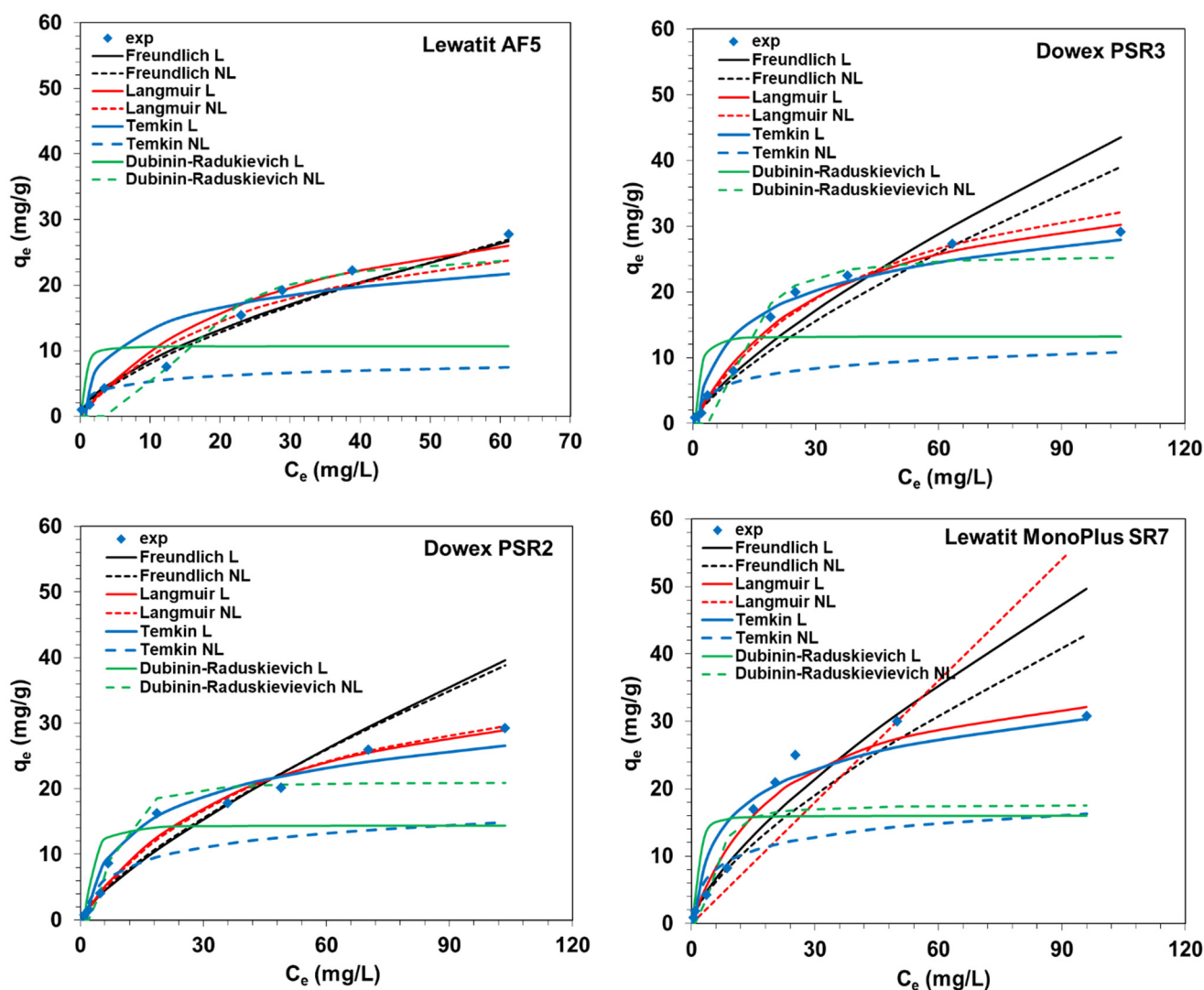


Figure 10. Examples of the isotherms fitting to the experimental data for the sorption of V(V) ions on SR7, PSR2, PSR3, and AF5 sorbents using L (linear) and NL (non-linear) regressions.

As follows from Table 5, the comparison of correlation coefficient  $R^2$  values obtained for the models shows that the Langmuir model fits well with the experimental data for S984, A830, and A400TL ( $R^2$  values range from 0.927 to 1.000). In the case of SR7, both Langmuir and Freundlich models produce similar values of  $R^2$  at 0.959 and 0.963, respectively, whereas for PSR2 and PSR3, the  $R^2$  values obtained based on the three isotherm Langmuir, Freundlich, and Temkin models are similar in the range from 0.940 to 0.954 for PSR2 and from 0.924 to 0.962 for PSR3. The Dubinin–Raduskievich isotherm model generally did not find applicability for the description of the V(V) adsorption on all sorbents under discussion. For AF5, the Freundlich isotherm model is the best fitting. Moreover, when the correlation coefficients for the Langmuir model are high, a high agreement between the adsorption capacity values obtained experimentally and those determined from the model can also be observed. Comparing the values of the adsorption capacities calculated based on the proper isotherm models included in Table 4 [4,11,17,36,46] and the other ion exchangers (e.g., the weakly basic anion exchange resins: 717 ( $q_{max} = 18.54$  mg/g), D314 ( $q_{max} = 18.08$  mg/g), D201 ( $q_{max} = 18.02$  mg/g), and 201\*7 ( $q_{max} = 48.0$  mg/g) [2] as well as the carbon adsorbents, e.g., sawdust biochar ( $q_{max} = 1.5$  mg/g), commercial activated carbon (AC) ( $q_{max} = 7.58$  mg/g), ZnCl<sub>2</sub>-corn straw biochar ( $q_{max} = 26.26$  mg/g), CsCl-corn straw biochar ( $q_{max} = 43.28$  mg/g), Zr(SO<sub>4</sub>)<sub>2</sub>-corn straw biochar ( $q_{max} = 58.74$  mg/g), ZnCl<sub>2</sub>-coir pith derived ( $q_{max} = 24.9$  mg/g), Norit ROY 0.8 AC ( $q_{max} = 37.87$  mg/g), etc.) [4], it can

be concluded that S984, A830, and A400TL are very promising in vanadium removal due to the exhibited largest adsorption capacities.

The adsorption mechanism of vanadium on different types of sorbents is different and depends strictly on the adsorbate and adsorbent type as well as the pH and experimental conditions of the adsorption process. The electrostatic interactions, ligand-exchange, ion-exchange, chelation, redox mechanism, or mixed interactions can be distinguished.

Electrostatic interactions proceed between anionic species of vanadium and the positively charged adsorbents. Depending on the solution's pH, the surface charge on the adsorbents can be changed as a result of the protonation and deprotonation of some surface functional groups. With the solution's pH increase, adsorbent surfaces tend to be more positively charged and stronger electrostatic attraction for the V anions can occur; e.g., the increased  $H^+$  ions concentration resulted in the protonation of the surface hydroxyl groups ( $-OH_2^+$ ) of the double-layered hydroxide-supported nanoscale zero-valent iron, leading to electrostatic attraction improvements [26]. On the other hand, electrostatic interactions could proceed between the cations, e.g.,  $Na^+$ ,  $Mg^{2+}$ ,  $Ca^{2+}$ , etc., adsorbed on the adsorbent surface, which form a bridge of a positive charge on the surface with the anionic vanadium species present in the solutions [52]. During the vanadium adsorption on the Ti-doped chitosan bead, the ligand exchange, electrostatic interaction, and redox reaction are the three main mechanisms responsible for vanadium adsorption ( $Ti^{4+}$  with the positive charge formed by the protonation results in stronger attraction towards the vanadium anions  $H_3V_2O_7^-$  or  $H_2VO_4^-$ ). The  $Cl^-$  ligand on the TiCB surface can also exchange with these anionic species and form the  $Ti-H_3V_2O_7$  or  $Ti-H_2VO_4$  complex; then, the surface of TiCB might be partially reduced, and the free V(IV) might be re-adsorbed to form the  $TiCB-V(IV)$  complex [53]. Kończyk et al. [4] suggested that the V(V) anions adsorbed onto BC2 biochar by the anion exchange, electrostatic interactions, H-bond formation mechanism, etc., and the functional groups of biochar participated in V adsorption. Moreover, the inner-sphere complexes' formation may occur during vanadium adsorption on iron-based materials [2].

In our studies, all sorbents, except for AF5, possess various quaternary ammonium or amine functional groups. They belong to strongly basic or weakly and weakly/chelating types of ion exchangers (see Table 1). On the other hand, the studies were carried out at pH 6 in acidic solutions (the forms of vanadium depending on its concentration and pH are included in Figure 2 in [11] and Figure 6a in this paper). For the anion exchange resin in form of  $Cl^-$ , ion exchange reactions can occur (see Equations (7)–(10)) [3,54]. Moreover, electrostatic interactions can proceed.

#### 2.4. Desorption Studies

Desorption of vanadium from the loaded sorbent (sorbent regeneration) and its reuse are an important factor influencing the practical application of sorbent and the total cost of the adsorption process. Vanadium is usually desorbed by various eluting agents, usually NaOH and HCl at various concentrations; e.g., vanadium is eluted from the SBA resins by 5% NaOH+10% NaCl (HZrO@ strongly basic anion exchanger D201, %D = 91.2%) [12], 6 mol/L HCl (D296 resin, %D = 98.68%) [8], 2 mol/L NaOH (Amberlite IRA400, %D = 57–72%, 30 min) [6], 2 mol/L NaOH (717, %D = 81.7%, 5 min) [55], or WBA resins by 3 mol/L NaOH (201\*7, %D > 95%) [56], 2% NaOH+10% NaCl (Dex-V, %D = 99.5%) [14], etc. In such solutions, the repulsion between the vanadium oxyanions and the sorbents as well as the electrostatic attractions ceases between the protonated functional groups and vanadium, resulting in easier vanadium desorption. However, in many cases, vanadium removal is not quantitative, and desorption yields depend on the eluting type, regeneration time, temperature, and the type of mechanism [2].

In vanadium desorptions from the S984, A830, A400TL, SR7, PSR2, PSR3, and AF5 sorbents, the 0.1, 0.25, 0.5, and 1 mol/L HCl and 0.1, 0.25, 0.5, and 1 mol/L NaOH solutions were applied as eluting agents under experimental conditions:  $W = 0.1 \pm 0.0005$  g,  $V = 20$  mL, pH 6, 170 rpm,  $A = 8$ ,  $T = 295$  K,  $t = 4$  h (Table 6).



**Table 6.** Vanadium desorption yield from S984, A830, A400TL, SR7, PSR2, PSR3, AF5.

	S984	A830	A400TL	SR7	PSR2	PSR3	AF5	
0.1 mol/L HCl	57.6	27.1	5.9	6.5	5.0	4.3	15.5	
0.25 mol/L HCl	85.8	42.7	15.0	6.1	5.7	2.4	11.0	
0.5 mol/L HCl	≈ 100%	59.1	26.0	7.4	8.8	6.1	11.2	
1 mol/L HCl		76.6	77.5	14.4	5.4	7.6	11.5	
0.1 mol/L NaOH		≈ 100%		45.5	66.6	6.4	58.8	11.5
0.25 mol/L NaOH				70.6	82.6	6.2	58.8	19.5
0.5 mol/L NaOH				99.9	84.2	7.0	60.4	26.8
1 mol/L NaOH				99.7	78.2	5.3	59.4	14.8

■ The largest desorption yield.

As observed, the desorption yield is changeable and depends on the eluting agent's concentration. The desorption from SR7, PSR2, PSR3, and AF5 using the HCl solution is not satisfactory, and usually the largest desorption yield was obtained using 0.5 or 1 mol/L HCl for SR7, PSR2, PSR3, and 0.1 mol/L HCl for AF5. In the case of vanadium desorption from S984, A830, and A400TL, the desorption yield using 1 mol/L HCl is above 77.5%. Improved desorption was obtained using NaOH solutions, mainly the 0.5 mol/L NaOH solution. For the WBA resin, the desorption yield by NaOH is normally higher (quantitative) compared to SBA (%D is in the range from 5.3 to 99.7%), which is consistent with the literature data [6,12,14,56].

### 2.5. Column Studies

The removal of contaminants in the continuous system is preferred in practical applications and is of great industrial importance. For this reason, the removal of vanadium from the solutions of its various initial concentrations (50, 100, and 200 mg/L) was conducted by the column method (pH 6, the solution flow rate through the bed was 0.4 mL/min). The eluate was collected in fractions of an appropriate volume until the initial concentration of V(V) ions was obtained. The column studies resulted in the determination of breakthrough curve (the ratio of V(V) concentrations in the aqueous solution ( $C$ ) with an initial concentration of V(V) ( $C_0$ ) versus the eluate volume ( $V$ )) (Figure 11) and then the column parameters such as the weight distribution coefficient ( $D_w$ ), the bed distribution coefficient ( $D_b$ ), and the working ion exchange capacity ( $C_w$ ) (g/mL) were determined (see Equations (4)–(6) in Table 2 and results in Table 7).

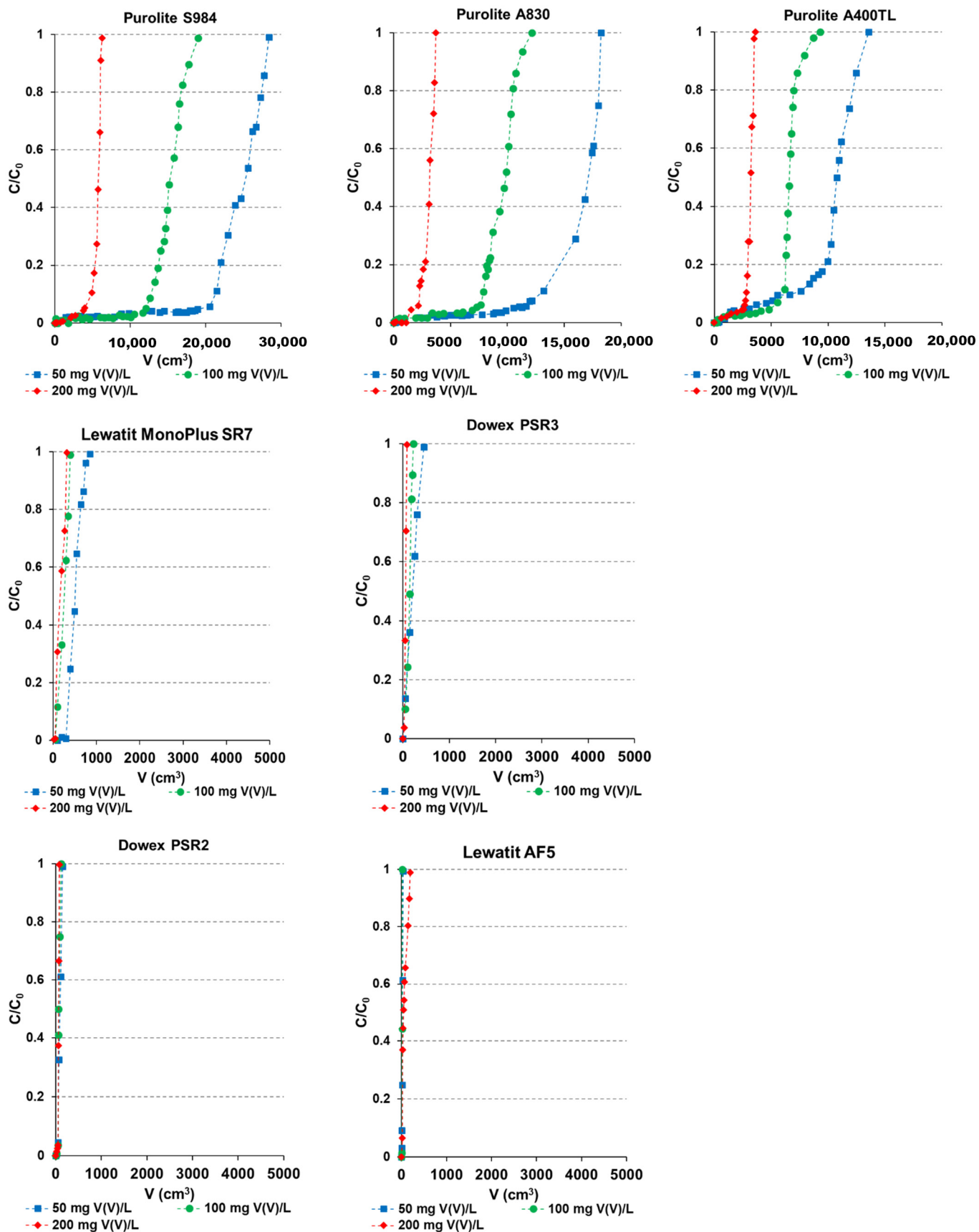


Figure 11. Breakthrough curves obtained during the adsorption of vanadium by the column studies.

**Table 7.** Column parameters obtained for the vanadium adsorption from the solutions of the initial concentrations 50, 100, and 200 mg/L.

Sorbent	$C_w$ (g/mL)	$D_w$	$D_v$
A830	3.5	4914.9	1710.4
	9.5	2831.6	985.4
	17.7	2629.0	914.9
A400TL	4.5	3172.7	1074.9
	8.0	1946.3	659.4
	12.0	940.7	318.7
S984	7.0	6755.4	2529.9
	23.0	4082.5	1528.9
	25.6	1543.9	578.2
SR7	1.0	190.7	50.7
	1.0	95.1	25.3
	1.0	59.8	15.9
PSR3	0.3	63.6	19.9
	0.5	44.7	14.0
	0.5	16.9	5.3
PSR2	0.1	22.0	8.5
	0.3	15.2	5.9
	0.4	15.0	5.8
AF5	0	3.6	2.1
	0	1.6	1.0
	0	7.2	4.2

As it was shown the breakthrough curves resembled the typical “S” shape in all cases. Moreover, the curve for the vanadium initial concentration 200 mg/L is steeper indicating that in this case the systems worked more efficiently. A reflection of this fact are the working ion exchange parameters values which increase with the increasing initial concentration and the highest values were obtained for the solutions of 200 mg V(V)/L. Based on the  $C_w$  the efficiency series of the sorbents under discussion towards V(V) are:

$C_0 = 50$  mg/L: S984 > A400TL > A830 > SR7 > PSR3 > PSR2 > AF5;

$C_0 = 100$  mg/L: S984 > A830 > A400TL > SR7 > PSR3 > PSR2 > AF5;

$C_0 = 200$  mg/L: S984 > A830 > A400TL > SR7 > PSR3 > PSR2 > AF5.

In all presented cases, the series are similar, indicating that for the AF5 sorbent being at the end of the series, column breakthrough occurs immediately after the adsorption process begins; therefore, the volume of the eluate collected to the breakthrough point is equal to 0, and the working ion exchange capacity is also zero. The weight and bed volume coefficients decrease with an increase in initial vanadium concentrations.

As it was found, S984, A830, and A400TL are the most efficient in vanadium removal by the column studies, which is consistent with the results obtained during equilibrium studies by means of the static method.

## 2.6. Removal of Vanadium from Real Wastewaters

The vanadium catalysts (4–9 wt%  $V_2O_5$  together with the alkali metal sulfate promoters: potassium sulfate or cesium sulfate on the silica carrier material) are used for sulfuric acid production. The catalyst’s life cycle is limited from seconds even up to 10 years of work and then such a catalyst becomes a spent one (containing  $VOSO_4$ ,  $(VO_2)_2SO_4$  and

V<sub>2</sub>O<sub>5</sub>) and can be either stored or processed to recover valuable metals [57,58]. The storage of spent catalysts requires appropriate conditions to protect them against weather conditions (the presence of sulfate, free sulphite, and water can result in an acidic leachate and environmental contamination) [57]. Therefore, the storage of spent catalysts is not environmentally acceptable, and their treatment by a simple process is preferable [59].

To study the sorbent's applicability for vanadium removal from real wastewater, the vanadium spent catalyst for sulfuric acid production was leached using 5% m/m HCl (R1), 5% m/m H<sub>2</sub>SO<sub>4</sub> (R2), and 15% m/m NaOH (R3), 15% m/m KOH (R4) ( $T = \text{ambient}$ ,  $t = 6 \text{ h}$ ,  $S:L = 1.5$ ). The characteristics of the real wastewater were previously described in [11]. After leaching, the content of V(V) was close to 5000 mg/L whereas that of Fe(III) was 50x higher in solutions obtained by digestion with the acid (1000 mg/L) than for the alkali ones ( $\approx 15\text{--}20 \text{ mg/L}$ ). After leaching, potassium, sodium, sulphur, chloride, silica, and copper(II) were also present in the solution.

It was found that the removal of V(V) and Fe(III) was the most effective by SR7, A400TL, PSR3, and PSR2 using 15% m/m KOH (R4) for spent catalyst digestion, whereas for WBA, resins (S984 and A830) V(V) and Fe(III) were the most efficiently removed from the R2 (5% m/m H<sub>2</sub>SO<sub>4</sub>) and R4 (15% m/m KOH) solutions, respectively. Lewatit AF5 did not reveal the applicability for V(V) removal, whereas the %R for Fe(III) was below 50.4% using alkali digestion agents. The largest removal of vanadium was obtained using the S984 ion exchanger (%R = 98%, R2), A830 (80.6%, R2), and A400TL (67.8%, R4). After pH adjustments to 5, in most cases, V(V) and Fe(III) removal efficiencies increased, and the precipitation of V(V) ions Fe(III) was observed in alkaline solutions.

### 3. Materials and Methods

#### 3.1. Reagents and Instruments

All chemical compounds (sodium metavanadate, NaVO<sub>3</sub>, acids: HNO<sub>3</sub>, HCl, H<sub>2</sub>SO<sub>4</sub>; alkalis: NaOH, KOH) were of analytical grade and were supplied by Merc KGaA (Darmstadt, Germany) or Avantor Performance Materials (Gliwice, Poland).

The weakly basic (Purolite A830), weakly basic/chelating (Purolite S984), and strongly basic (Lewatit MonoPlus SR7, Purolite A400TL, Dowex PSR2, Dowex PSR3) ion exchangers and microporous Lewatit AF5 sorbents without the functional groups were purchased from Purolite International Co, Dow Chemical Company (Philadelphia, PA, USA) or Lanxess (Cologne, Germany). The sorbents were pre-treated before use and converted to the Cl<sup>-</sup> form where necessary. The specifications of the sorbents under discussion are presented in Table 1.

The Fourier transform infrared spectra of the frequency range from 650 to 4000 cm<sup>-1</sup> were obtained using the Attenuated Total Reflectance Fourier Transform Infrared Spectroscopy (ATR-FTIR) analysis by means of the Cary 630 instrument (Agilent Technologies, Santa Clara, CA, USA) and the Agilent MicroLab PC software (version: B.04) using the diamond attachment at a spectral resolution 4 cm<sup>-1</sup> and the measurement time 30 s. The band intensities were expressed in transmittance (%T).

The SEM images of the sorbents were obtained using the Quanta<sup>TM</sup> 3D FEG microscope with the EDS (Energy Dispersive Spectroscopy)/EBSD (Electron Backscatter Diffraction) system (Hillsboro, OR, USA).

The specific surface area ( $S_{BET}$ ), the total pore volumes ( $P_v$ ) and the average pore size ( $P_s$ ) were obtained by the Brunauer–Emmett–Teller method and by means of the ASAP 2405 analyzer (Micromeritics Instrument Corporation, Norcross, GA, USA).

All adsorption tests by the static method were carried out using the laboratory Elpin+ shaker type 358A (Lubawa, Poland).

After the adsorption process, V(V) concentrations in the solution were determined at a wavelength of 318.5 nm by applying the four-step time-temperature program (slit width 0.2 nm, lamp current 10 mA) by means of the Graphite Furnace Atomic Absorption Spectrometry (GF-AAS) and Varian AA240Z (Melbourne, Australia) spectrometer equipped with the graphite furnace tube GTA120.

### 3.2. Batch and Column Studies—Experimental Conditions

The vanadium(V) adsorption was conducted by means of static (batch) and dynamic (column) methods.

In the batch method, in the conical flasks with a 100 mL volume closed with a silicone stopper, 20 mL of V(V) solution of the initial concentrations at 50 mg/L (effect of pH, adsorbent dose), 5–200 mg/L (kinetic studies), 5–2000 mg/L (equilibrium studies), and 0.01–0.1 g (effect of adsorbent dose) (0.1, 0.5 g (effect of pH), or 0.1 g (others)) of the sorbent was placed. Then, Erlenmeyer flasks were inserted in a mechanical shaker operation at the vibration amplitude of 8 units and 170 cycles per minute at 295K and mixed from 1 min to 24 h (kinetic studies) for 4h (effect of pH, adsorbent dose, desorption) or 24 h (equilibrium studies). The details of experimental conditions are listed in Figure 12.

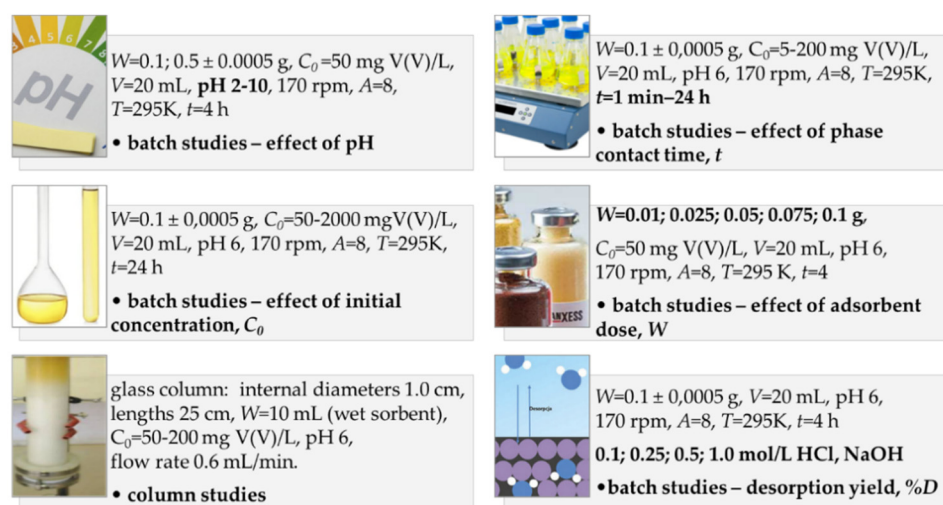


**Figure 12.** Experimental parameters applied in the vanadium(V) adsorption.

Then, the sorbent was separated from the solution, and the concentration of V(V) was measured using the GF-AAS method. Next the percentage removal (%R) (Equation (1)), the amount of V(V) adsorbed after time  $t$  ( $q_t$ ) (Equation (2)), and sorption capacity ( $q_e$ ) (Equation (3)) were calculated (Table 2).

Dynamic adsorption experiments were conducted in glass columns of the internal diameters equal to 1.0 cm and 25 cm in length. The columns were packed with the wet sorbent of 10 mL volume and then loaded with V(V) solutions of the initial concentrations 50, 100, and 200 mg/L and pH 6 at a flow rate 0.4 mL/min. The samples of proper volume were collected to determine the V(V) concentration and to obtain breakthrough curves. Then, the column parameters such as the weight ( $D_w$ ) (Equation (4)) and bed ( $D_b$ ) (Equation (5)) distribution coefficients as well as the working ion exchange capacity ( $C_w$ ) (Equation (6)) were calculated (Table 2).

The V(V) adsorption results were analyzed using kinetic models: the pseudo-first order kinetic equation (PFO), the pseudo-second order kinetic equation (PSO), the intraparticle diffusion (IPD) (Equations (11)–(15)) (kinetic studies results), or the isotherm ones—Langmuir, Freundlich, Temkin, and Dubinin–Raduskievich (Equations (16)–(25)) (equilibrium studies results).

The error functions such as the chi-square test ( $\chi^2$ ) and the sum of squares of the errors (SSE) were applied for kinetic data analyses according to the equations presented in [60]:

$$\chi^2 = \sum_{i=1}^n \frac{(q_{e \text{ exp}} - q_{e \text{ cal}})^2}{q_{e \text{ exp}}} \quad (26)$$

$$SSE = \sum_{i=1}^n (q_{e \text{ exp}} - q_{e \text{ cal}})^2 \quad (27)$$



where  $q_{e,exp}$  (mg/g)—the experimental values of amount of V(V) adsorbed at equilibrium;  $q_{e,cal}$  (mg/g)—the calculated amount of V(V) adsorbed.

#### 4. Conclusions

In this study, the process of V(V) ion removal on the weakly basic (Purolite A830), weakly basic/chelating (Purolite S984), and strongly basic (Lewatit MonoPlus SR7, Purolite A400TL, Dowex PSR2, Dowex PSR3) ion exchange resins and the microporous Lewatit AF5 sorbent without functional groups using the static and column methods was investigated. The effects of pH, adsorbent dose, phase contact time, initial V(V) ions concentration on the V(V) adsorption efficiency, and the type and concentration of eluting agents on the desorption yield were discussed. In addition, the efficiency of V(V) and Fe(III) ions removal from real wastewater as a result of leaching of spent vanadium catalysts used in the production of sulfuric acid is presented. It was shown that the above mentioned parameters affect both the adsorption and desorption of V(V) ions on/from the tested sorbents significantly. The optimum pH and the sorbent's dose were 6 and 0.1 g, respectively. Experimental adsorption data are well described by the PSO model and the Langmuir, Freundlich, or Temkin isotherm models. The obtained maximum experimental capacities (221.4 mg/L for S984, 202 mg/L for A830, and 200.4 mg/L for A400TL), working ion exchange capacities (25.6 g/mL for S984, 17.7 g/mL for A830, 12 g/mL for A400TL,  $C_0 = 200$  mg/L), the desorption efficiency (close to 100% using NaOH), and real wastewaters treatment for S984 (%R = 98%, R2), A830 (80.6%, R2), and A400TL (67.8%, R4) show that these ion exchangers can be promising in practical applications for vanadium(V) removal and vanadium containing wastewater treatment on a larger scale.

**Author Contributions:** Conceptualization, A.W.; methodology, A.W.; validation, A.W.; formal analysis, A.W.; investigation, A.W.; software, A.W.; writing—original draft preparation, A.W., Z.H.; writing—review and editing, A.W. and Z.H.; visualization, A.W. All authors have read and agreed to the published version of the manuscript.

**Funding:** This paper was supported by the National Science Centre Poland under research project no. 2018/29/B/ST8/01122.

**Institutional Review Board Statement:** Not applicable.

**Informed Consent Statement:** Not applicable.

**Data Availability Statement:** The data presented in this study are available in this article.

**Acknowledgments:** The authors thank Gabriela Giza and Alicja Opala for their contributions in some obtained experimental results.

**Conflicts of Interest:** The authors declare no conflict of interest.

**Sample Availability:** Samples of the compounds are not available from the authors.

#### References

1. Lee, J.-C.; Kim, E.Y.; Chung, K.W.; Kim, R.; Jeon, H.S. A review on the metallurgical recycling of vanadium from slags: Towards a sustainable vanadium production. *J. Mater. Res. Technol.* **2021**, *12*, 343–364. [[CrossRef](#)]
2. Liu, J.; Huang, Y.; Li, H.; Duan, H. Recent advances in removal techniques of vanadium from water: A comprehensive review. *Chemosphere* **2022**, *287*, 132021. [[CrossRef](#)] [[PubMed](#)]
3. Peng, H.; Guo, J.; Li, B.; Huang, H.; Shi, W.; Liu, Z. Removal and recovery of vanadium from waste by chemical precipitation, adsorption, solvent extraction, remediation, photo-catalyst reduction and membrane filtration. A review. *Environ. Chem. Lett.* **2022**, *20*, 1763–1776. [[CrossRef](#)]
4. Kończyk, J.; Kluziak, K.; Kołodziejka, D. Adsorption of vanadium(V) ions from the aqueous solutions on different biomass-derived biochars. *J. Environ. Manag.* **2022**, *313*, 114958. [[CrossRef](#)] [[PubMed](#)]
5. Polowczyk, I.; Cyganowski, P.; Urbano, B.F.; Rivas, B.L.; Bryjak, M.; Kabay, N. Amberlite IRA-400 and IRA-743 chelating resins for the sorption and recovery of molybdenum(VI) and vanadium(V): Equilibrium and kinetic studies. *Hydrometallurgy* **2017**, *169*, 496–507. [[CrossRef](#)]
6. Gomes, H.I.; Jones, A.; Rogerson, M.; Greenway, G.M.; Lisbona, D.F.; Burke, I.T.; Mayes, W.M. Removal and recovery of vanadium from alkaline steel slag leachates with anion exchange resins. *J. Environ. Manag.* **2017**, *187*, 384–392. [[CrossRef](#)]

7. Zhu, X.; Li, W.; Zhang, Q.; Zhang, C.; Chen, L. Separation characteristics of vanadium from leach liquor of red mud by ion exchange with different resins. *Hydrometallurgy* **2018**, *176*, 42–48. [[CrossRef](#)]
8. Hu, J.; Wang, X.; Xiao, L.; Song, S.; Zhang, B. Removal of vanadium from molybdate solution by ion exchange. *Hydrometallurgy* **2009**, *95*, 203–206. [[CrossRef](#)]
9. Zeng, L.; Li, Q.G.; Xiao, L.S. Extraction of vanadium from the leach solution of stone coal using ion exchange resin. *Hydrometallurgy* **2009**, *97*, 194–197. [[CrossRef](#)]
10. Li, W.; Zhang, Y.; Liu, T.; Huang, J.; Wang, Y. Comparison of ion exchange and solvent extraction in recovering vanadium from sulfuric acid leach solutions of stone coal. *Hydrometallurgy* **2013**, *131*, 1–7. [[CrossRef](#)]
11. Wołowicz, A.; Hubicki, Z. Removal of vanadium by ion exchange resins from model and real solutions from spent V<sub>2</sub>O<sub>5</sub> catalyst. *Hydrometallurgy* **2022**, *211*, 105871. [[CrossRef](#)]
12. Li, Q.G.; Zeng, L.; Xiao, L.S.; Yang, Y.N.; Zhang, Q.X. Completely removing vanadium from ammonium molybdate solution using chelating ion exchange resins. *Hydrometallurgy* **2009**, *98*, 287–290. [[CrossRef](#)]
13. Fang, H.X.; Li, H.Y.; Xie, B. Effective chromium extraction from chromium containing vanadium slag by sodium roasting and water leaching. *ISIJ Int.* **2012**, *52*, 1958–1965. [[CrossRef](#)]
14. Li, H.Y.; Li, C.; Zhang, M.; Wang, K.; Xie, B. Removal of V(V) from aqueous Cr(VI)-bearing solution using anion exchange resin: Equilibrium and kinetics in batch studies. *Hydrometallurgy* **2016**, *165*, 381–389. [[CrossRef](#)]
15. Wołowicz, A.; Hubicki, Z. Enhanced Removal of Copper(II) from Acidic Streams Using Functional Resins: Batch and Column Studies. *J. Mater. Sci.* **2020**, *55*, 13687–13715. [[CrossRef](#)]
16. Prekob, Á.; Hajdu, V.; Muránszky, G.; Kocserha, I.; Fiser, B.; Viskolcz, B.; Vanyorek, L. Application of carbonized ion exchange resin beads as catalyst support for gas phase hydrogenation processes. *React. Kinet. Mech. Catal.* **2020**, *129*, 85–94. [[CrossRef](#)]
17. Burdzy, K.; Chen, Y.-G.; Lv, G.-Y.; Chen, S.-H.; Kołodyńska, D. Application of Ion Exchangers with the N-Methyl-D-Glucamine Groups in the V(V) Ions Adsorption Process. *Materials* **2022**, *15*, 1026. [[CrossRef](#)]
18. Ezzeldin, H.A.; Apblett, A.; Foutch, G.L. Synthesis and properties of anion exchangers derived from chloromethyl styrene codivinylbenzene and their use in water treatment. *Int. J. Polym. Sci.* **2010**, *2010*, 684051. [[CrossRef](#)]
19. Humelnicu, D.; Dragan, E.S. Evaluation of phosphate adsorption by porous strong base anion exchangers having hydroxyethyl substituents: Kinetics, equilibrium, and thermodynamics. *Environ. Sci. Pollut. Res.* **2021**, *28*, 7105–7115. [[CrossRef](#)]
20. Kim, J.; Park, C.W.; Lee, K.-W.; Lee, T.S. Adsorption of Ethylenediaminetetraacetic Acid on a Gel-Type Ion-Exchange Resin for Purification of Liquid Waste Containing Cs Ions. *Polymers* **2019**, *11*, 297. [[CrossRef](#)]
21. Application Note 50829, Carbon Black Analysis Using FT-IR with Germanium and Diamond ATR. Available online: [thermoscientific.com](https://www.thermoscientific.com) (accessed on 20 August 2022).
22. Wołowicz, A.; Hubicki, Z. Carbon-based adsorber resin Lewatit AF 5 applicability in metal ion recovery. *Microporous Mesoporous Mater.* **2016**, *224*, 400–414. [[CrossRef](#)]
23. Fan, C.; Chen, N.; Qin, J.; Yang, Y.; Feng, C.; Li, M.; Gao, Y. Biochar stabilized nano zero-valent iron and its removal performance and mechanism of pentavalent vanadium(V(V)). *Colloids Surf. A Physicochem. Eng. Asp.* **2020**, *599*, 124882. [[CrossRef](#)]
24. Keränen, A.; Leiviskä, T.; Salakka, A.; Tanskanen, J. Removal of nickel and vanadium from ammoniacal industrial wastewater by ion exchange and adsorption on activated carbon. *Desalination Water Treat.* **2013**, *53*, 2645–2654. [[CrossRef](#)]
25. Leiviskä, T.; Matusik, J.; Muir, B.; Tanskanen, J. Vanadium removal by organo-zeolites and iron-based products from contaminated natural water. *J. Clean. Prod.* **2017**, *167*, 589–600. [[CrossRef](#)]
26. Kong, X.; Chen, J.; Tang, Y.; Lv, Y.; Chen, T.; Wang, H. Enhanced removal of vanadium(V) from groundwater by layered double hydroxide-supported nanoscale zerovalent iron. *J. Hazard. Mater.* **2020**, *392*, 122392. [[CrossRef](#)]
27. Greenwood, N.N.; Earnshaw, A. 22-Vanadium, Niobium and Tantalum. In *Chemistry of the Elements*, 2nd ed.; Butterworth-Heinemann: Oxford, UK, 1997; pp. 976–1001. [[CrossRef](#)]
28. Guzmán-Pantoja, J.; Saucedo, I.; Navarro, R.; Revilla, J.; Guibal, E. Vanadium Interactions with Chitosan: Influence of Polymer Protonation and Metal Speciation. *Langmuir* **2002**, *18*, 1567–1573. [[CrossRef](#)]
29. Dorsey, B.M.; McLauchlan, C.C.; Jones, M.A. Evidence That Speciation of Oxovanadium Complexes Does Not Solely Account for Inhibition of Leishmania Acid Phosphatases. *Front. Chem.* **2018**, *6*, 109. [[CrossRef](#)]
30. Peacock, C.L.; Sherman, D.M. Vanadium(V) adsorption onto goethite ( $\alpha$ -FeOOH) at pH 1.5 to 12: A surface complexation model based on ab initio molecular geometries and EXAFS spectroscopy. *Geochim. Cosmochim. Acta* **2004**, *68*, 1723–1733. [[CrossRef](#)]
31. Livage, J. Hydrothermal Synthesis of Nanostructured Vanadium Oxides. *Materials* **2010**, *3*, 4175–4195. [[CrossRef](#)]
32. Bello, A.; Leiviskä, T.; Zhang, R.; Tanskanen, J.; Maziarz, P.; Matusik, J.; Bhatnagar, A. Synthesis of zerovalent iron from water treatment residue as a conjugate with kaolin and its application for vanadium removal. *J. Hazard. Mater.* **2019**, *374*, 372–381. [[CrossRef](#)]
33. Wołowicz, A.; Wawrzekiewicz, M.; Hubicki, Z. Toxic heavy metal ions and metal-complex dyes removal from aqueous solutions using an ion exchanger and titanium dioxide. *Fibres Text. East. Eur.* **2018**, *26*, 108–115. [[CrossRef](#)]
34. Li, M.; Zhang, B.; Zou, S.; Liu, Q.; Yang, M. Highly selective adsorption of vanadium(V) by nano-hydrous zirconium oxide-modified anion exchange resin. *J. Hazard. Mater.* **2020**, *384*, 121386. [[CrossRef](#)] [[PubMed](#)]
35. Zhang, R.; Leiviskä, T. Surface modification of pine bark with quaternary ammonium groups and its use for vanadium removal. *Chem. Eng. J.* **2020**, *385*, 123967. [[CrossRef](#)]

36. Gomes, H.I.; Jones, A.; Rogerson, M.; Burke, I.T.; Mayes, W.M. Vanadium removal and recovery from bauxite residue leachates by ion exchange. *Environ. Sci. Pollut. Res.* **2016**, *23*, 23034–23042. [[CrossRef](#)]
37. Pyrzyńska, K.; Wierzbicki, T. Pre-concentration and separation of vanadium on Amberlite IRA-904 resin functionalized with porphyrin ligands. *Anal. Chim. Acta.* **2005**, *540*, 91–94. [[CrossRef](#)]
38. Zhu, X.; Li, W.; Zhang, C. Extraction and removal of vanadium by adsorption with resin 201\*7 from vanadium waste liquid. *Environ. Res.* **2020**, *180*, 108865. [[CrossRef](#)]
39. Chen, B.; Bao, S.X.; Zhang, Y.M.; Zheng, R.W. A high-efficiency approach for the synthesis of N235-impregnated resins and the application in enhanced adsorption and separation of vanadium(V). *Minerals* **2018**, *8*, 358. [[CrossRef](#)]
40. Zheng, R.W.; Bao, S.X.; Zhang, Y.M.; Chen, B. Synthesis of di-(2-ethylhexyl) phosphoric acid (D2EHPA)-Tributyl phosphate (TBP) impregnated resin and application in adsorption of vanadium(IV). *Minerals* **2018**, *8*, 206. [[CrossRef](#)]
41. Lagergren, S.K. About the theory of so-called adsorption of soluble substances. *Sven. Vetenskapsakad. Handlingar* **1898**, *24*, 1–39.
42. Ho, Y.S.; McKay, G. Pseudo-second order model for sorption processes. *Process Biochem.* **1999**, *34*, 451–465. [[CrossRef](#)]
43. Weber, W.J.; Morris, J.C. Kinetics of adsorption on carbon from solution. *J. Sanit. Eng. Div.* **1963**, *89*, 31–60. [[CrossRef](#)]
44. Stanisz, M.; Klapiszewski, Ł.; Kołodyńska, D.; Jesionowski, T. Development of functional lignin-based spherical particles for the removal of vanadium(V) from an aqueous system. *Inter. J. Biol. Macromol.* **2021**, *186*, 181–193. [[CrossRef](#)] [[PubMed](#)]
45. Kajjumba, G.W.; Aydın, S.; Güneysu, S. Adsorption isotherms and kinetics of vanadium by shale and coal waste. *Adsorp. Sci. Technol.* **2018**, *36*, 936–952. [[CrossRef](#)]
46. Gurjar, V.R.; Koujalagi, P.S.; Revankar, H.N.; Kulkarni, R.M. Adsorptive removal of vanadium from aqueous media by ion exchange resin. *Emerg. Mater.* **2021**. [[CrossRef](#)]
47. Langmuir, I. The adsorption of gases on plane surfaces of glass, mica and platinum. *J. Am. Chem. Soc.* **1918**, *40*, 1361–1403. [[CrossRef](#)]
48. Freundlich, H.M.F. Over the adsorption in solution. *J. Phys. Chem.* **1906**, *57*, 385–471.
49. Wawrzkiwicz, M.; Wołowicz, A.; Hubicki, Z. Strongly Basic Anion Exchange Resin Based on a Cross-Linked Polyacrylate for Simultaneous, C.I. Acid Green 16, Zn(II), Cu(II), Ni(II) and Phenol Removal. *Molecules* **2022**, *27*, 2096. [[CrossRef](#)]
50. Temkin, M.I.; Pyzhev, V. Kinetics of ammonia synthesis on promoted iron catalysts. *Acta Physicochim. URSS* **1940**, *12*, 327–356.
51. Redlich, O.; Peterson, D.L. A useful adsorption isotherm. *J. Phys. Chem.* **1959**, *63*, 1024. [[CrossRef](#)]
52. Zhu, H.W.; Xiao, X.Y.; Guo, Z.H.; Han, X.Q.; Liang, Y.Q.; Zhang, Y.; Zhou, C. Adsorption of vanadium(V) on natural kaolinite and montmorillonite: Characteristics and mechanism. *Appl. Clay Sci.* **2018**, *161*, 310–316. [[CrossRef](#)]
53. Liu, X.; Zhang, L. Insight into the adsorption mechanisms of vanadium(V) on a high-efficiency biosorbent (Ti-doped chitosan bead). *Int. J. Biol. Macromol.* **2015**, *79*, 110–117. [[CrossRef](#)] [[PubMed](#)]
54. Zeng, L.; Cheng, C.Y. A literature review of the recovery of molybdenum and vanadium from spent hydrodesulphurisation catalysts Part II: Separation and purification. *Hydrometallurgy* **2009**, *98*, 10–20. [[CrossRef](#)]
55. Huang, J.; Su, P.; Wu, W.; Liao, S.; Qin, H.; Wu, X.; He, X.; Tao, L.; Fan, Y. Concentration and separation of vanadium from alkaline media by strong alkaline anion-exchange resin 717. *Rare Met.* **2010**, *29*, 439–443. [[CrossRef](#)]
56. Zhao, Z.; Li, X.; Zhao, Q. Recovery of V<sub>2</sub>O<sub>5</sub> from Bayer liquor by ion exchange. *Rare Met.* **2010**, *29*, 117–120. [[CrossRef](#)]
57. Mangini, L.F.K.; Valt, R.B.G.; de Santana Ponte, M.J.J.; de Araújo Ponte, H. Vanadium removal from spent catalyst used in the manufacture of sulfuric acid by electrical potential application. *Sep. Purif. Technol.* **2020**, *246*, 116854. [[CrossRef](#)]
58. Mohanty, J.; Rath, P.C.; Bhattacharya, I.N.; Paramguru, R.K. The recovery of vanadium from spent catalyst: A case study. *Miner. Process. Extr. Metall.* **2011**, *120*, 56–60. [[CrossRef](#)]
59. Park, K.H.; Mohapatra, D.; Reddy, B.R. Selective recovery of molybdenum from spent HDS catalyst using oxidative soda ash leach/carbon adsorption method. *J. Hazard. Mater.* **2006**, *138*, 311–316. [[CrossRef](#)]
60. Popoola, L.T. Characterization and adsorptive behaviour of snail shell-rice husk (SS-RH) calcined particles (CPs) towards cationic dye. *Heliyon* **2019**, *5*, e01153. [[CrossRef](#)] [[PubMed](#)]